iScience

CellPress
OPEN ACCESS

Article

The nucleolus functions as the compartment for histone H2B protein degradation

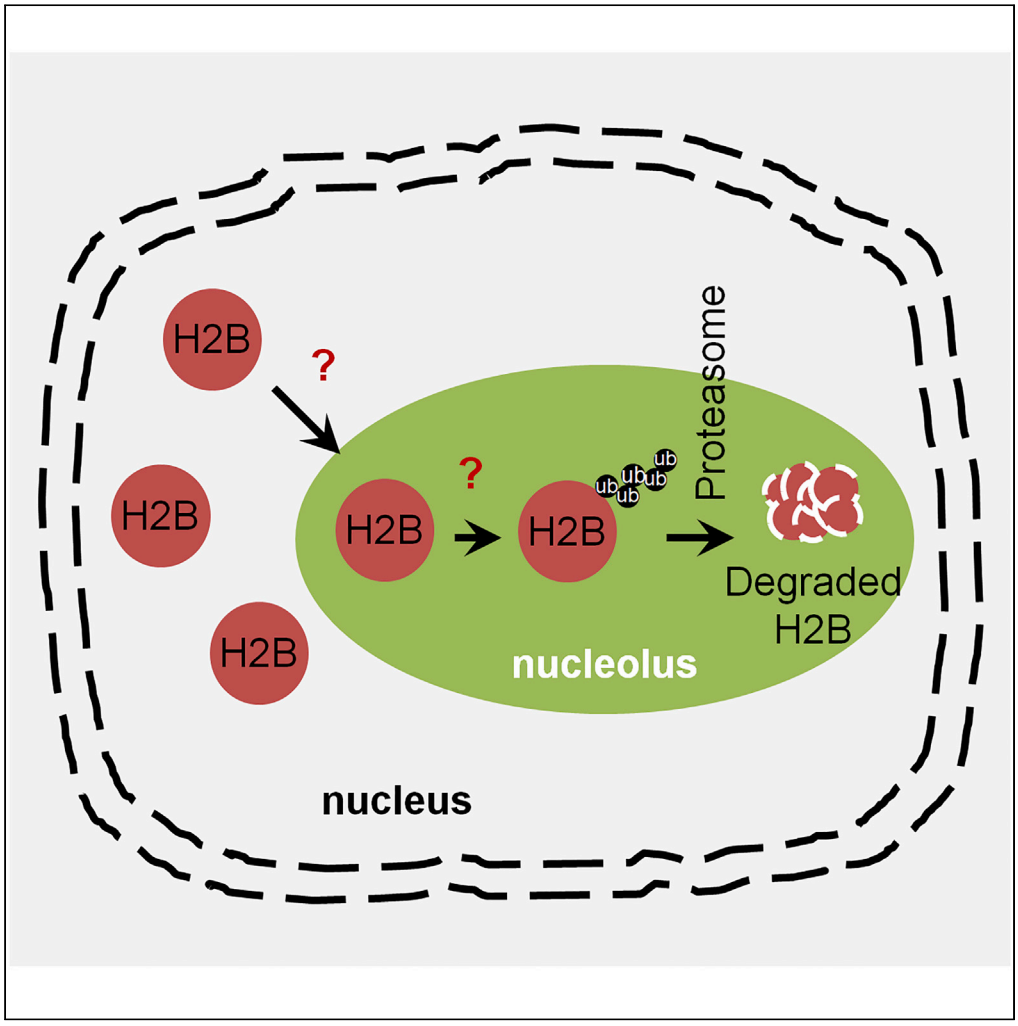

Yanping Liu, Yufei Wang, Lu Yang, ..., Xiaojun Zhang, Wen Cui, Su Chen

kjk6915252@126.com (X.Z.)
cuiwenmd@163.com (W.C.)
chensu@xjtu.edu.cn (S.C.)

HIGHLIGHTS

Histone H2B can be polyubiquitinated at the lysine 120 residue

The degradation of histone H2B is achieved via the ubiquitination-proteasome pathway

The nucleolus regulates the protein degradation of histone H2B

Liu et al., iScience *24*, 102256
April 23, 2021
https://doi.org/10.1016/j.isci.2021.102256

iScience

CellPress
OPEN ACCESS

Article

The nucleolus functions as the compartment for histone H2B protein degradation

Yanping Liu,[1,6] Yufei Wang,[1,6] Lu Yang,[1,6] Feng Sun,[2,6] Sheng Li,[3,6] Yequan Wang,[3] Guo-An Zhang,[3] Tingting Dong,[3] Lei-Lei Zhang,[3] Wanglin Duan,[1] Xiaojun Zhang,[4,*] Wen Cui,[3,*] and Su Chen[1,3,4,5,7,*]

SUMMARY

Histones are main components of chromatin, and the protein levels of histones significantly affect chromatin assembly. However, how histone protein levels are regulated, especially whether and how histones are degraded, is largely unclear. Here, we found that histone H2B is mainly degraded through the proteasome-mediated pathway, and the lysine-120 site of H2B is essential for its K48-linked polyubiquitination and degradation. Moreover, the degradation-impaired H2BK120R mutant shows an increased nucleolus localization, and inhibition of the proteasome results in an elevated nucleolus distribution of wild-type H2B, which is similar to that of H2BK120R mutants. More importantly, the nucleolus fractions can ubiquitinate and degrade the purified H2B *in vitro*, suggesting that the nucleolus, in addition to its canonical roles regulating ribosome genesis and protein translation, likely associates with H2B degradation. Therefore, these findings revealed a novel mechanism for the regulation of H2B degradation in which a nucleolus-associated proteasome pathway is involved.

INTRODUCTION

In eukaryotes, approximately 147 base pairs of genomic DNA wrap around a core histone octamer containing two copies of H2A, H2B, H3, and H4 to form a nucleosome. The nucleosome is the basic structural unit of genetic materials, and the assembly and disassembly of nucleosomes significantly affect gene transcription (Luger et al., 1997). Accumulating studies have indicated that all histones can be catalyzed with various covalent modifications, including ubiquitination, methylation, acetylation, phosphorylation, sumoylation, and ADP ribosylation (Strahl and Allis, 2000). Moreover, investigations about histone modifications are still the hot spot in the field of epigenetics, as recently, several new types of histone modifications, such as propionylation, butyrylation, crotonylation, 2-hydroxyisobutyrylation, malonylation, succinylation, acylation, lipidation, monoaminylation, and glycation, have been identified (Huang et al., 2014; Chan and Maze, 2020). Each modification shows nonnegligible impacts on the corresponding histones, or the higher order chromatin organization, or even gene transcription (Chi et al., 2010). The amount of histones significantly affects chromatin structure, gene transcription, and many other biological processes. For instance, in the testis, histones are replaced by transition proteins and subsequently by protamines during spermatogenesis to accommodate gene expression and development (Mills et al., 1977; Hammoud et al., 2009). In addition, histones are diminished at the promoter regions or gene body regions of activated genes in somatic cells under specific conditions (Dion et al., 2007; Deal et al., 2010). However, the mechanisms underlying the alterations of histone dosages remain unknown (Chen and Qiu, 2012).

Protein ubiquitination is a sequential ATP-dependent enzymatic process that is catalyzed by E1 ubiquitin-activating enzyme, E2 ubiquitin-conjugating enzyme, and E3 ubiquitin-protein ligase (Lu and Hunter, 2009; Bassermann et al., 2014). Ubiquitination can be classified into two types: monoubiquitination and polyubiquitination. Protein polyubiquitination is formed through the internal lysine residues (K6, K11, K27, K29, K33, K48, and K63) or the N-terminal methionine of ubiquitin (Clague and Urbé, 2010; Behrends and Harper, 2011). K48- or K11-linked polyubiquitination usually destines the substrates to be degraded by the 26S proteasome, whereas monoubiquitination or K63-linked polyubiquitination results in various nonproteolytic outcomes for the substrates (Bassermann et al., 2014). Histones have been identified to be monoubiquitinated. For example, monoubiquitination of histone H2A and H2B have been extensively

[1]Laboratory of Molecular and Cellular Biology, School of Forensic Sciences, Xi'an Jiao Tong University Health Science Center, Xi'an, Shaanxi 710061, PR China

[2]Research Center for Translational Medicine at East Hospital, School of Life Sciences and Technology, Tongji University, Shanghai, Shanghai 200092, PR China

[3]School of Forensic Sciences and Laboratory Medicine, Jining Medical University, Jining, Shandong 272067, PR China

[4]Department of Science and Education, People's Hospital of Zunhua, Tangshan, Hebei 064200, PR China

[5]Laboratory of Molecular and Cellular Biology, School of Basic Medical Sciences, Henan University School of Medicine, Kaifeng, Henan 475004, PR China

[6]These authors contributed equally

[7]Lead contact

*Correspondence: kjk6915252@126.com (X.Z.), cuiwenmd@163.com (W.C.), chensu@xjtu.edu.cn (S.C.)

https://doi.org/10.1016/j.isci.2021.102256

studied and have been reported to be associated with chromatin structure organization, transcriptional regulation, and DNA repair (Zhang, 2003; Weake and Workman, 2008; Cao and Yan, 2012). However, whether eukaryotic histones can be polyubiquitinated and degraded and how the protein levels of histones are controlled are poorly understood. A recent study revealed that in eukaryotes, RNF8 mediates the K48-linked polyubiquitination of histone H3 and further results in the protein degradation of H3 via the 26S proteasome pathway (Xia et al., 2017). However, how the protein levels of other histones, such as H2B, are controlled is still unknown.

In this study, we demonstrated that histone H2B is mainly degraded through the 26S proteasome pathway, and the lysine 120 residue of H2B is essential for H2B protein degradation. Mutation of lysine 120 to arginine (K120R) blocked the K48-linked polyubiquitination and resulted in an elevated nucleolus localization. Inhibition of the proteasome activity also led to an obvious nucleolus distribution of wild-type H2B, which is similar to that of H2BK120R mutants. Moreover, the isolated nucleolus fractions could ubiquitinate and degrade the purified H2B *in vitro*, suggesting that the nucleolus is likely associated with H2B protein degradation.

RESULTS

Histone H2B is degraded through the 26S proteasome pathway

To know whether H2B can be degraded, various inhibitors for the two well-defined protein degradation pathways were employed. MG132 was used to block the 26S proteasome-mediated protein degradation pathway, whereas Bafilomycin A1 (BafA1) and 3-MA were used to block the autophagy-lysosome-mediated protein degradation pathway. The results indicated that histone H2B can indeed be degraded, and the degradation of H2B is mainly occurred through the 26S proteasome-mediated pathway, as only blocking the 26S proteasome activity resulted in the accumulation of H2B protein levels significantly, whereas inhibition of the autophagy-lysosome pathway showed no obvious effect on H2B protein levels (Figure 1A). Our result is partially consistent to previous studies, as histone H3 and H4 were reported to be degraded through the 26S proteasome pathway during DNA damage response in yeast (Hauer et al., 2017), and human H3 is also degraded through the 26S proteasome pathway, which is regulated by RNF8 (Xia et al., 2017). In addition, we also tested the effects of the protein degradation inhibitors used above on cell wellness, including examinations of cell morphology, cell apoptosis, and cell cycle progression. We found that no obvious cell death morphology was observed after the treatment of these drugs (Figure S1A). Only slight changes on cell-cycle progression were observed in MG132-treated 293T cells. The percentage of G1 phase cells was slightly decreased (about 9%), whereas the percentage of G2/M phase cells was slightly increased (about 8%) (Figure S1B). Although the percentages of G1 and G2/M phase cells were slightly affected by MG132 treatment, the percentage of S phase cells (the change of S phase may affect histone protein levels) likely was not affected by MG132. In addition, slight increases of apoptosis were detected in Baf A1- and 3-MA-treated 293T cells (Figure S1C). However, Baf A1 and 3-MA does not affect H2B protein levels (Figure 1A). Therefore, these data suggested that the accumulation of H2B protein levels induced by MG132 treatment is likely not due to its effects on cell cycle and cell wellness.

Lysine 120 of histone H2B is essential for H2B protein degradation

To determine which lysine is essential for H2B degradation, multiple lysine residues were mutated to arginine (both generated based on the sequence of H2BE and data not shown), and H2B half-life was determined with chase assays. Wild-type H2B (H2BWT) and lysine residue-mutated H2B-transfected HEK293T cells were pretreated with cycloheximide (CHX), which blocks protein synthesis, for distinct time points. Our results indicated that the lysine 120 residue of histone H2B is required for H2B protein degradation, as wild-type H2B (both endogenous H2B- and GFP-tagged H2BWT) was degraded with a half-life time of approximately 8 h, whereas the degradation of the lysine-120-mutated H2B (H2BK120R) was completely blocked (Figures 1B and S2). Consistently, H2BK120R showed higher protein levels than H2BWT (Figure 1C, left), when equal amounts of H2BWT and H2BK120R constructs were transfected into HEK293T cells, whereas their mRNA levels were comparable (Figure 1C, right), supporting that a posttranscriptional mechanism may be involved in the observed difference between the H2BWT and H2BK120R protein levels. Consistent with the previous findings, our results revealed that MG132 treatment increased the H2BWT protein levels to a comparable level as the H2BK120R mutants, suggesting that MG132 treatment eliminated the difference between H2BWT and H2BK120R protein levels (Figure 1D). This result indicated that the observed lower protein levels of H2BWT than H2BK120R are mainly due to the 26S proteasome-mediated protein degradation of H2BWT.

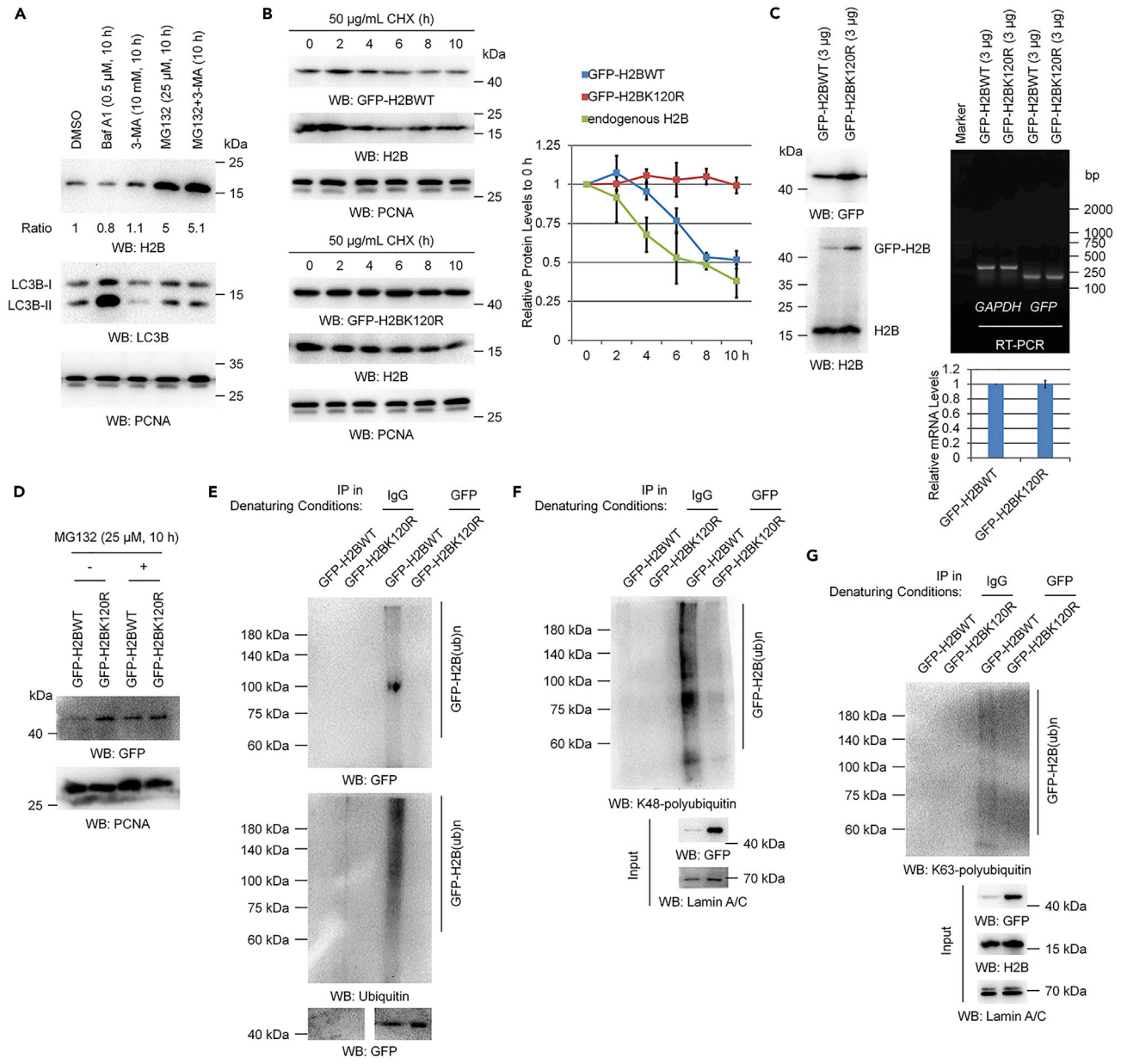

Figure 1. The K120 residue of H2B is essential for the degradation and polyubiquitination of H2B

(A) 293T cells were treated with Baf A1 (0.5 μM), 3-MA (10 mM), or MG132 (25 μM) separately or in combination as indicated for 10 h. DMSO treatment was used as the control group. Western blot assays were then performed with antibodies as indicated. PCNA was used as the internal control.

(B) Western blot analysis of 293T cells transfected with a GFP-H2BWT or a GFP-H2BK120R plasmid and treated with 50 μg/mL Cycloheximide (CHX) for the indicated time points. PCNA was used as the internal control. The bands were semiquantified by ImageJ (right).

(C) Western blot (left) and RT-PCR (right) analyses of 293T cells transfected with equal amounts of GFP-H2BWT or GFP-H2BK120R plasmids. Endogenous H2B (for western blot analysis) and GAPDH (for RT-PCR analysis) were used as the internal controls. The RT-PCR bands were semiquantified by ImageJ (lower).

(D) Western blot analyses of 293T cells transfected with equal amounts of GFP-H2BWT or GFP-H2BK120R plasmids and further treated with (+) or without (–) 25 μM MG132 for 10 h. PCNA was used as the internal control.

(E–G) Protein ubiquitination analysis was performed in 293T cells transfected with equal amounts of the GFP-H2BWT or GFP-H2BK120R plasmids. Antibodies against ubiquitin, K48-linked polyubiquitin, and K63-linked polyubiquitin were used as indicated.

All the experiments were repeated more than three times, similar results were obtained, and representative images were provided. Bars and error bars are the mean ± s.d., n = 3 independent repeats.

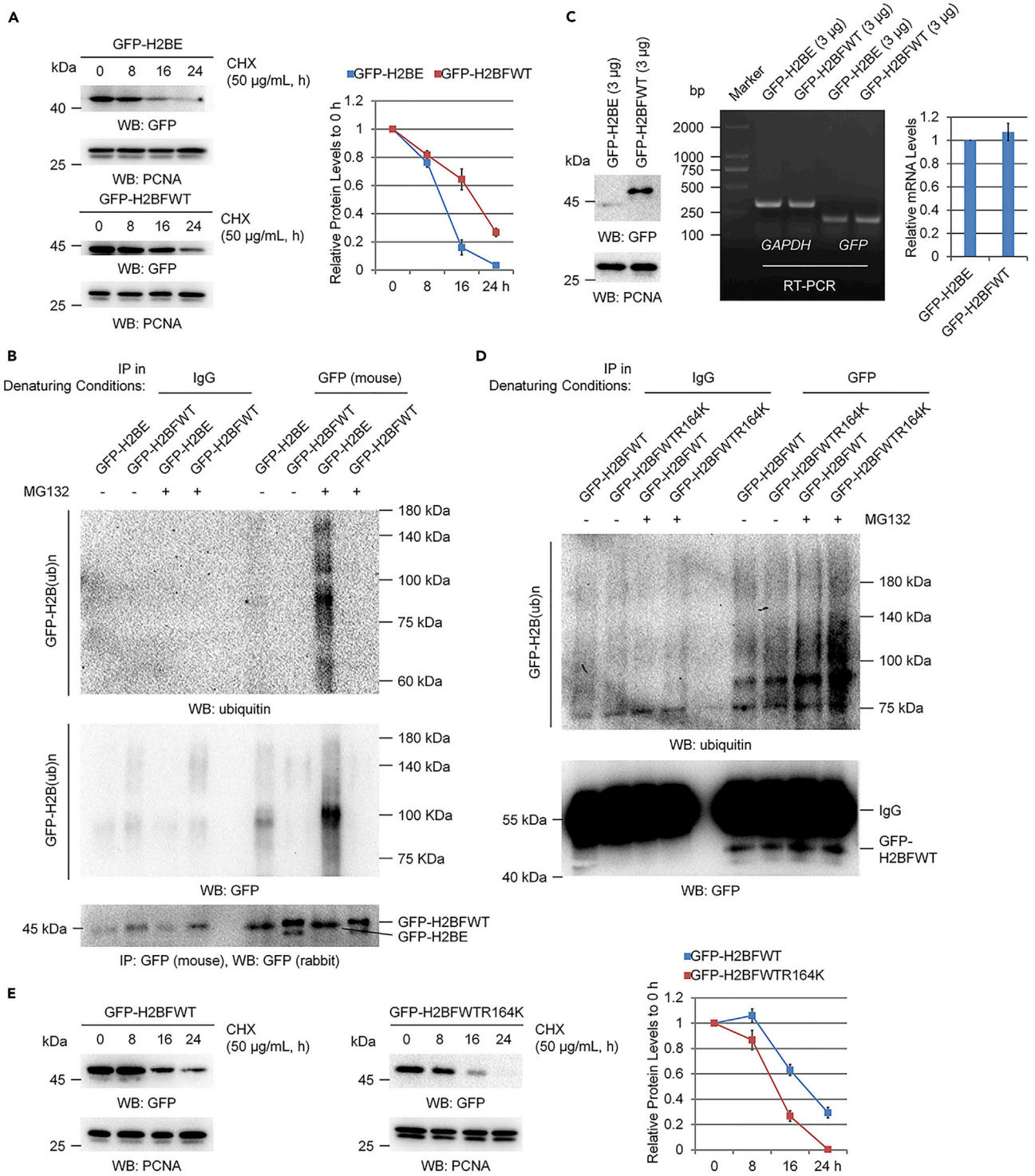

Figure 2. H2BFWT is more stable than H2BE

(A) Western blot analysis of 293T cells transfected with a GFP-tagged H2BE (GFP-H2BE) or a GFP-tagged H2BFWT (GFP-H2BFWT) plasmid and treated with 50 μg/mL CHX for the indicated time points. PCNA was used as the internal control. The bands were semiquantified by ImageJ (right).

(B) Protein ubiquitination analysis was performed in 293T cells transfected with equal amounts of the GFP-H2BE or GFP-H2BFWT plasmids and treated with (+) or without (–) 25 μM MG132 for 10 h as indicated.

Figure 2. *Continued*

(C) Western blot (left) and RT-PCR (right) analyses of 293T cells transfected with equal amounts of the GFP-H2BE or GFP-H2BFWT plasmids. PCNA (for western blot analysis) and GAPDH (for RT-PCR analysis) were used as the internal controls. The RT-PCR bands were semiquantified by ImageJ (right, lower).

(D) Protein ubiquitination analysis was performed in 293T cells transfected with equal amounts of the GFP-tagged wild-type H2BFWT (GFP-H2BFWT) or GFP-tagged R164K-mutated H2BFWT (GFP-H2BFWTR164K) plasmids and treated with (+) or without (–) 25 μM MG132 for 10 h as indicated.

(E) Western blot analysis of 293T cells transfected with a GFP-H2BFWT or a GFP-H2BFWTR164K plasmid and treated with 50 μg/mL CHX for the indicated time points. PCNA was used as the internal control. The bands were semiquantified by ImageJ (right).

All the experiments were repeated more than three times, similar results were obtained, and representative images were provided. Bars and error bars are the mean ± s.d., n = 3 independent repeats.

In line with these results supporting 26S proteasome-dependent degradation of histone H2B, we found that H2B was indeed polyubiquitinated, whereas mutation of the lysine 120 residue to arginine almost completely abolished the polyubiquitination of H2B, suggesting that the observed polyubiquitination likely occurred on the K120 residue (Figure 1E). More interestingly, in accordance with the differential roles of K48- and K63-linked polyubiquitination as mentioned earlier, our results determined that H2B is mainly ubiquitinated with a K48-linked polyubiquitination, which may be tightly related to its protein degradation, whereas only weak K63-linked polyubiquitination was observed (Figures 1F and 1G). Together, these results suggested that H2B is likely polyubiquitinated at the K120 residue mainly with a K48-linked polyubiquitination form, and this K48-linked polyubiquitination further promotes the 26S proteasome-dependent H2B protein degradation.

H2BFWT (the homologous lysine 120 residue is naturally mutated to arginine) is more stable than H2BE

We also aligned multiple H2B isoforms in both human and mouse, and intriguingly, we found that, in the testis of both human and mouse, there is a natural K to R mutation of the conserved residue corresponding to lysine 120 (H2BFWT in human and H2B subacrosomal variant in mouse) (Figure S3). This result suggested that the modification of this site may be tightly restricted in some biological processes and also provided a rationality for the K120 to R mutation used in this study. As indicated in Figure S3A, human H2BFWT shows an intrinsic substitution at the lysine 120 homologous site with an arginine residue (R164). We therefore examined the differences in protein stability between these two proteins. As expected, H2BFWT with an intrinsic R residue at the K120 homologous site (R164) showed a prolonged half-life time, suggesting that H2BFWT is more stable than H2BE (Figure 2A). We also tested the polyubiquitination levels of H2BE and H2BFWT. Consistent with the differential protein degradation rate, H2BFWT showed lower polyubiquitination levels than H2BE (almost undetectable in H2BFWT) (Figure 2B). Finally, we compared the exact protein levels of H2BE and H2BFWT in 293T cells transfected with equal amounts of plasmids. As expected, higher protein levels of H2BFWT were detected than that of H2BE (Figure 2C, left), whereas the mRNA levels between H2BE and H2BFWT were comparable (Figure 2C, right), further confirming the above notion that H2BFWT is more stable than H2BE.

To further support the key role of the K120 homologous residue in the control of H2B protein stability, we next reversely mutated the K120 homologous residue of H2BFWT (R164) to a lysine (H2BFWTR164K) to test whether the mutated H2BFWTR164K protein can be polyubiquitinated. Intriguingly, we found that more polyubiquitination occurred on H2BFWTR164K than on wild-type H2BFWT (Figure 2D), and an increased protein degradation rate was also observed in the H2BFWTR164K mutant (Figure 2E). Together, these data indicated that the K120 homologous residue is critical for H2B protein polyubiquitination and degradation.

Mutation of the K120 residue of H2B to R results in a nucleolus accumulation of H2B

We accidentally examined the localization of wild-type H2BE (GFP-H2BWT) and K120R-mutated H2BE (GFP-H2BK120R). Intriguingly, a typically dotted distribution in the nucleus of H2BK120R-mutated proteins was observed, whereas wild-type H2B showed a dispersed distribution in the nucleus with relative lack of staining in the corresponding H2BK120R dotted positions (Figure 3A). To further identify the compartment accumulated by H2BK120R-mutated proteins, we double stained H2B and H2BK120R with a nucleolus marker, nucleolin (NCL). As expected, we found that H2BK120R-mutated proteins colocalized well with NCL, and the empty vacuoles in wild-type H2B distribution also corresponded to NCL (Figure 3B), suggesting that the mutated H2BK120R proteins accumulated in the nucleolus. To further validate that H2BK120R-mutated proteins accumulate in the nucleolus, we differentially isolated the nucleolus and other cellular

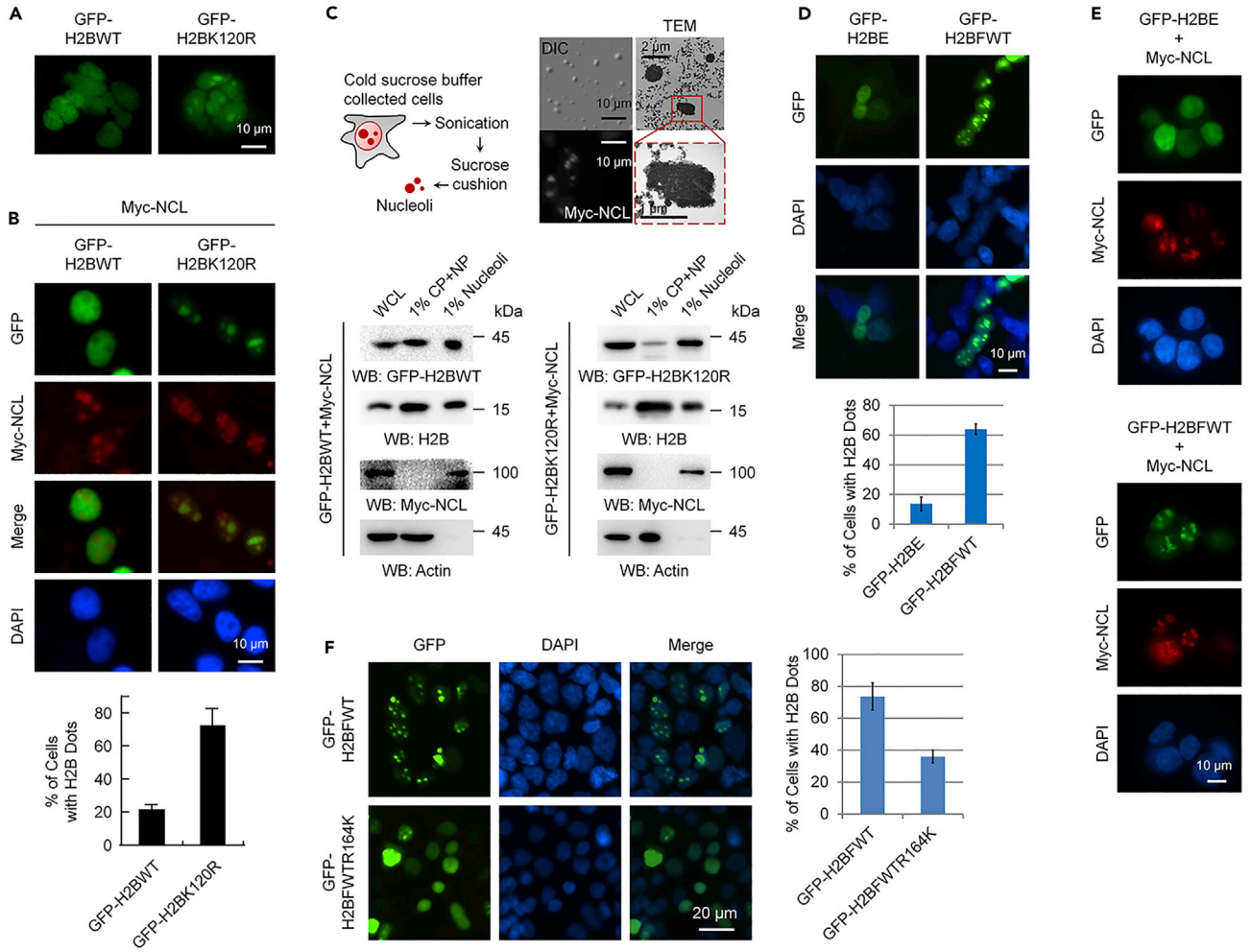

Figure 3. K120R-mutated H2Bproteins show an obvious nucleolus distribution

(A) Fluorescence microscopy analysis of 293T cells transfected with a GFP-H2BWT or a GFP-H2BK120R construct.

(B) Immunofluorescence (IF) assay for 293T cells transfected with a Myc-tagged nucleolin (Myc-NCL) plasmid together with a GFP-H2BWT or a GFP-H2BK120R plasmid. The percentage of cells with H2B dots in the nucleolus was calculated (lower). More than 500 cells were counted in each group.

(C) Nucleolus isolation followed by western blot analysis was performed in 293T cells transfected with a GFP-H2BWT or a GFP-H2BK120R construct together with a Myc-NCL plasmid. The isolated nucleoli were also photographed with a differential interference contrast (DIC) microscope and a transmission electron microscope (TEM), and the nuclei stained with antibodies against NCL were also shown to compare the size of isolated nucleoli (upper, right).

(D) Fluorescence microscopy analysis of 293T cells transfected with a GFP-H2BE or a GFP-H2BFWT construct. The percentage of cells with H2B dots was calculated (lower). More than 500 cells were counted in each group.

(E) IF assay for 293T cells transfected with a Myc-tagged nucleolin (Myc-NCL) plasmid together with a GFP-H2BE or a GFP-H2BFWT plasmid to determine the nucleolus distribution of the dotted H2B.

(F) Fluorescence microscopy analysis of 293T cells transfected with a GFP-H2BFWT or a GFP-H2BFWTR164K construct. The percentage of cells with H2B dots was calculated (right).

All the experiments were repeated more than three times, similar results were obtained, and representative images were provided. Bars and error bars are the mean ± s.d., n = 3 independent repeats.

compartments with a previously reported method (Liang et al., 2012; Li and Lam, 2015). Our data indicated that both endogenous H2B and ectopically expressed wild-type H2B (GFP-H2BWT) showed relatively higher amounts in the non-nucleoli fractions, whereas H2BK120R-mutated proteins were predominantly distributed in the nucleoli fractions (Figure 3C), which is consistent with the results of the immunofluorescence assays (Figures 3A and 3B). We also compared the distribution of H2BE and H2BFWT, and similar to the H2BK120R mutant, H2BFWT also showed an obvious dotted localization (Figure 3D), and the dots were also corresponding to the nucleolus compartment (Figure 3E). Moreover, upon reversely mutating the R164

residue (the corresponding K120 homologous site of H2BFWT) to a lysine, the nucleolus distribution of H2BFWT was largely diminished (Figure 3F), further supporting the key role of the K120 homologous site in the control of H2B nucleolus accumulation.

The nucleolus is associated with H2B protein degradation

Increasing studies have indicated that, in addition to its canonical roles in the regulation of ribosome biogenesis, the nucleolus also plays critical roles in the control of protein degradation (Song and Wu, 2005; Tao et al., 2013; Guan et al., 2016). Together with our findings that the K120R-mutated H2B shows an obvious nucleolus distribution (Figures 3A–3C) and that the K120 residue is critical for H2B polyubiquitination and protein degradation (Figures 1B–1G and S2), we speculated that the nucleolus also participates in the regulation of H2B protein degradation. If the nucleolus is the compartment for H2B protein degradation, an obvious nucleolus distribution of H2B should appear upon inhibition of protein degradation. We therefore examined the effect of different protein degradation inhibitors on the distribution of wild-type H2B, and as expected, treatment with the proteasome inhibitor MG132 markedly increased the nucleolus distribution of both GFP-tagged wild-type H2B (Figure 4A) and endogenous H2B (Figure 4B), which is also in parallel with the observation that only MG132 abolished the protein degradation of wild-type H2B (Figures 1A and 1D). The nucleoli isolation followed by western blot analyses also supported the finding that blocking the proteasome activity by MG132 treatment results in an obvious nucleolus accumulation of both GFP-tagged wild-type H2B (Figure 4C) and endogenous H2B (Figure 4D). It is worth mentioning that, together with the finding that MG132 treatment resulted in an increase in H2B total protein levels (Figures 1A, 1D, 4C, and 4D, WCL lane), that the increase in H2B protein levels occurred in the nucleolus fraction (Figures 4C and 4D, Nucleoli lane), and that no obvious changes in the H2B protein levels were observed in other fractions (Figures 4C and 4D, CP + NP lane), these data suggested that the accumulation of H2B in the nucleolus is probably due to an impaired protein degradation by MG132 treatment, but not as a result of the redistribution of H2B in the nucleus, and that the nucleolus might be the compartment corresponding for H2B degradation. Furthermore, the degradation-strengthened H2BFWTR164K-mutated proteins also reshowed a nucleolus accumulation pattern upon MG132 treatment (Figure 4E), similar to the distribution of wild-type H2BFWT. Thus, these results suggested that the protein degradation activity of H2B tightly correlates with the nucleolus localization of H2B, and a nucleolus-related pathway might be involved in the regulation of H2B protein degradation.

To further verify the roles of the nucleolus in the regulation of H2B protein degradation, we next examined whether normal nucleolus activity is required for H2B nucleolus accumulation. Actinomycin D (Act D) was used to disrupt the normal nucleolus activity (Frottin et al., 2019). Intriguingly, we found that Act D treatment remarkably abolished the nucleolus accumulation of both wild-type H2B induced by MG132 and K120R-mutated H2B (Figure 4F). The effectiveness of Act D was also determined by immunostaining the nucleolus marker NCL. In Myc-NCL-transfected 293T cells, we found that Act D treatment disrupted the normal distribution of Myc-NCL, suggesting that the treatment of Act D under our conditions was functional and indeed destroyed the normal nucleolus activity (Figure S4A). These data suggested that normal nucleolus activity is likely required for the stable residence of H2B protein in the nucleolus waiting for degradation. In addition, it has been reported that the cysteine protease Calpain3 is essential for digestive organ expansion factor (Def)-mediated p53 degradation through a nucleolus-related protein degradation pathway that is independent on the ubiquitination and proteasome activity (Tao et al., 2013; Guan et al., 2016). However, a previous report revealed that the nucleolus-mediated Survivin-deltaEx3 (a functional splice variant of Survivin) is also degraded through the ubiquitination-proteasome pathway (Song and Wu, 2005). Although our data suggested that H2B degradation mediated by the nucleolus is likely through the ubiquitination-proteasome pathway, as MG132 treatment efficiently resulted in the clear accumulation of H2B protein levels and retention of H2B in the nucleolus (Figures 1A, 1D, and 4A–4D), to further test whether cysteine protease is also involved in H2B protein degradation, we therefore examined the effect of cysteine protease inhibitor ALLN on H2B protein levels. However, no obvious changes in H2B protein levels were observed upon ALLN treatment (Figure S4B). Thus, the protein degradation of H2B is likely achieved via a novel nucleolus-related protein degradation mechanism in a ubiquitination-proteasome pathway-dependent manner. In addition, as H2B can be monoubiquitinated by RNF20/RNF40 complex (Kim et al., 2005; Zhu et al., 2005) and RNF8 (Wu et al., 2009), we next examined whether these enzymes affect the protein levels and localization of H2B. By knocking down the expression of these enzymes (Figures S5A, S5D, and S5G), we found that these enzymes showed no obvious effects on both the protein levels and localization of H2B (Figures S5B–S5C, S5E, S5F, and S5H–S5I).

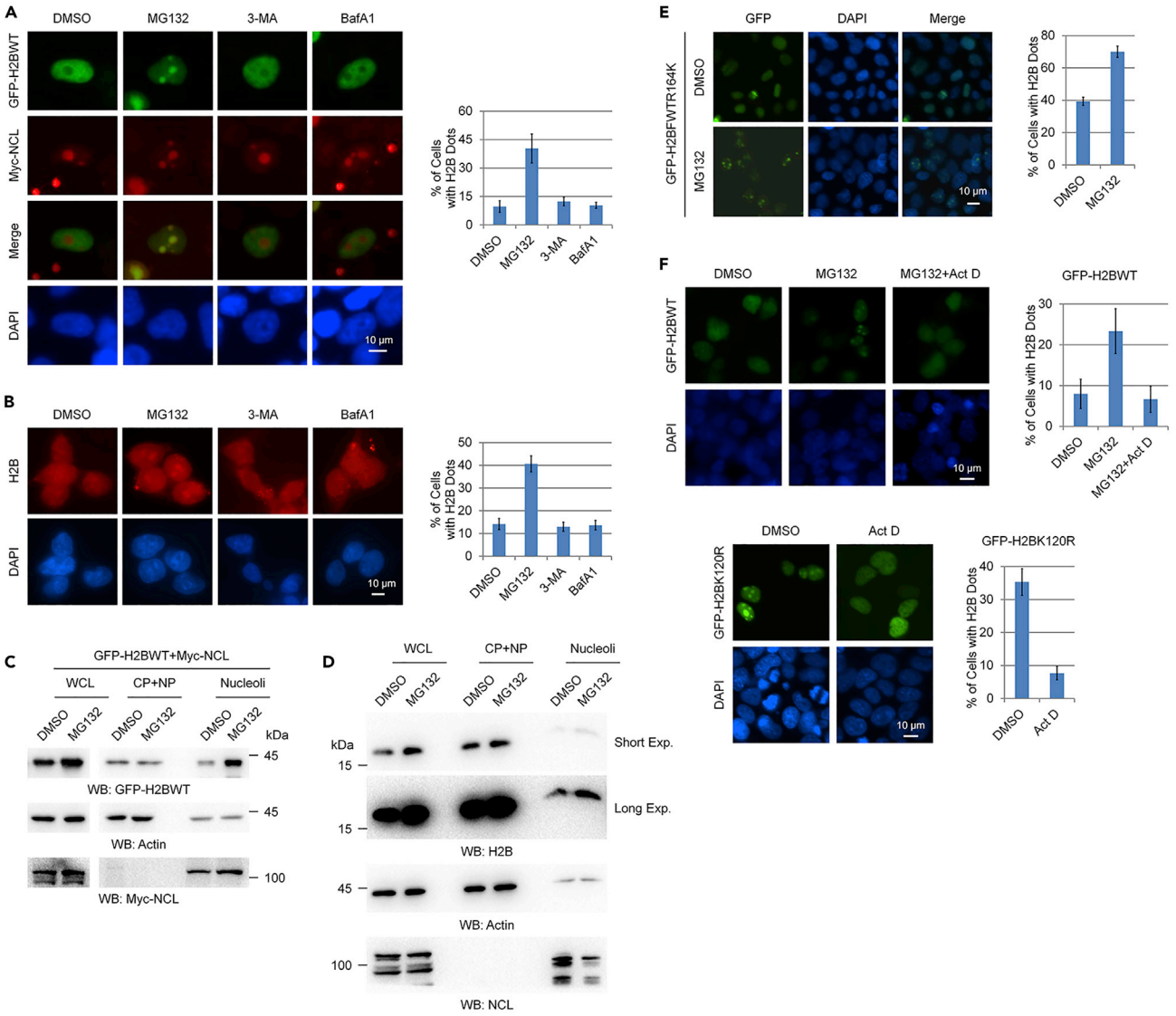

Figure 4. Inhibition of proteasome activity resulted in nucleolus accumulation of H2B

(A) IF analysis of 293T cells transfected with a GFP-H2BWT plasmid and a Myc-NCL plasmid and further treated with MG132 (25 μM), 3-MA (10 mM), or BafA1 (0.5 μM) for 10 h, as indicated. The percentage of cells with H2B dots in the nucleolus was calculated (right). More than 500 cells were counted in each group.

(B) IF analysis for 293T cells treated with 25 μM MG132, 10 mM 3-MA, or 0.2 μM BafA1 for 10 h, as indicated with H2B antibodies. The percentage of cells with H2B dots was calculated (right). More than 500 cells were counted in each group.

(C) Nucleolus isolation followed by western blot analysis was performed in 293T cells transfected with a GFP-H2BWT construct together with a Myc-NCL plasmid and treated with DMSO or 25 μM MG132 for 10 h, as indicated.

(D) Nucleolus isolation followed by western blot analyses was performed in 293T cells treated with DMSO or 25 μM MG132 for 10 h, as indicated.

(E) Fluorescence microscopy analysis of 293T cells transfected with a GFP-H2BFWTR164K plasmid and treated with DMSO or 25 μM MG132 for 10 h, as indicated. The percentage of cells with H2B dots was calculated (right). More than 500 cells were counted in each group.

(F) Fluorescence microscopy analysis of 293T cells transfected with a GFP-H2BWT or a GFP-H2BK120R plasmid and treated with 25 μM MG132 or 100 ng/mL actinomycin D (Act D) separately or in combination for 10 h, as indicated. The percentage of cells with H2B dots was calculated (right). More than 500 cells were counted in each group.

All the experiments were repeated more than three times, similar results were obtained, and representative images were provided. Bars and error bars are the mean ± s.d., n = 3 independent repeats.

Moreover, we also tested the effect of MG132 on the protein levels and localizations of other core histones including H2A, H3, and H4. We found that, similar as H2B, all the tested core histones showed increased protein levels after MG132 treatment (Figure S6A), which are consistent with previous reports that multiple

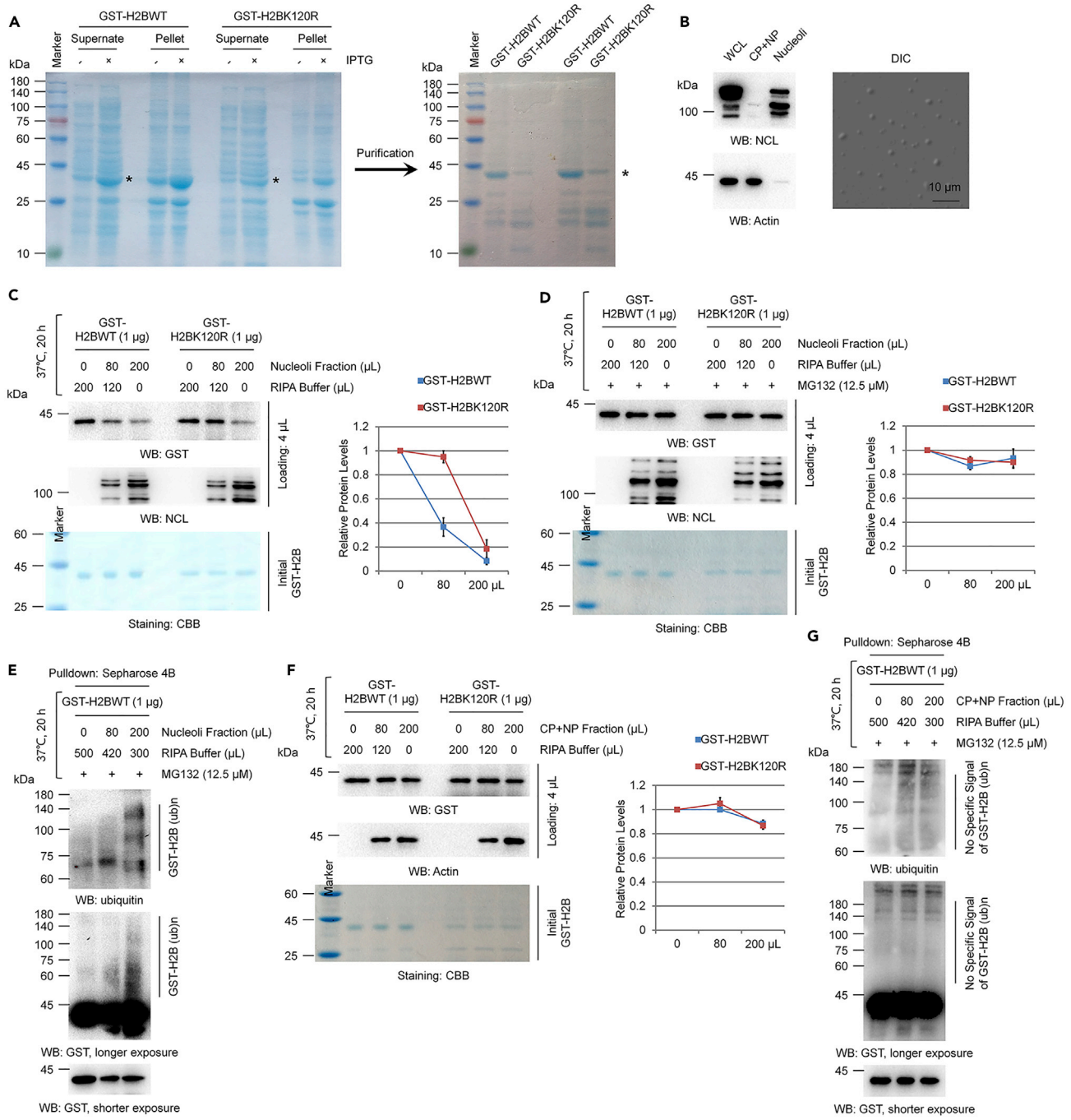

Figure 5. Nucleolus fractions ubiquitinate and degrade H2B *in vitro*

(A) Expression and purification of GST-tagged wild-type H2B (GST-H2BWT) and K120R-mutated H2B (GST-H2BK120R) in bacterial *E. coli*.

(B) Western blot and microscopy photograph (DIC) analyses for the isolated nucleoli fractions and non-nucleoli fractions (cytoplasm + nucleoplasm, CP + NP).

(C and D) *In vitro* GST-H2B degradation analysis by the nucleoli fractions. Reaction systems were established as indicated with equal amounts of GST-H2BWT or GST-H2BK120R proteins (1 μg) together with increased amounts of nucleoli extracts. MG123 was used (D) or not (C) to block the proteasome activity. The reaction systems were incubated at 37°C for 20 h. Samples were then subjected to western blot analyses. Coomassie bright blue (CBB) staining and NCL were used as the loading controls for GST-H2B and nucleoli extracts, respectively.

(E) *In vitro* GST-H2B ubiquitination analysis by the nucleoli fractions. Reaction systems were established as indicated with equal amounts of GST-H2BWT proteins (1 μg) together with increased amounts of nucleoli extracts. MG123 was used to block the proteasome activity. The reaction systems were incubated at 37°C for 20 h. Samples were pulled down by Sepharose 4B beads and then subjected to western blot analyses.

Figure 5. *Continued*

(F) *In vitro* GST-H2B degradation analysis by the non-nucleoli (CP + NP) fractions. Reaction systems were established as indicated with equal amounts of GST-H2BWT or GST-H2BK120R proteins (1 μg) together with increased amounts of non-nucleoli extracts. The reaction systems were incubated at 37°C for 20 h. Samples were then subjected to western blot analyses. CBB staining and actin were used as the loading controls for GST-H2B and non-nucleoli extracts, respectively.

(G) *In vitro* GST-H2B ubiquitination analysis by the non-nucleoli (CP + NP) fractions. Reaction systems were established as indicated with equal amounts of GST-H2BWT proteins (1 μg) together with increased amounts of non-nuclei extracts. MG123 was used to block the proteasome activity. The reaction systems were incubated at 37°C for 20 h. Samples were pulled down by Sepharose 4B beads and then subjected to western blot analyses.

All the experiments were repeated more than three times, similar results were obtained, and representative images were provided. Bars and error bars are the mean ± s.d., n = 3 independent repeats.

core histones are degraded through the proteasome pathway (Hauer et al., 2017; Xia et al., 2017). Moreover, an increased nucleolus distribution of H4 was observed after MG132 treatment (Figure S6B), whereas only very weak increases were observed in H2A and H3, although no statistical changes was detected upon MG132 treatment (Figures S6C and S6D), suggesting that distinct mechanisms may be involved in the regulation of histone degradation.

To further verify the functions of the nucleolus in the control of histone H2B protein degradation, we next examined the effects of the nucleolus on H2B protein degradation and ubiquitination in a cell-free system (*in vitro*). We first expressed and purified GST-tagged wild-type H2B (GST-H2BWT) and GST-tagged K120R-mutated H2B (GST-H2BK120R) from *Escherichia coli* (Figure 5A), and then the nucleolus fraction and non-nucleolus fraction (cytoplasm and nucleoplasm fraction, CP + NP) were differentially isolated (Figure 5B). The different cellular fractions were incubated with the purified GST-tagged H2B proteins to determine their effects on GST-H2B protein degradation and ubiquitination. To our surprise, in support to our *in vivo* data, we found that the nucleolus fractions could degrade GST-H2B *in vitro* (Figure 5C), whereas the cytoplasm and nucleoplasm fractions showed weak effects (Figure 5F). Moreover, in consistent with our *in vivo* data that the H2BK120R mutation impaired the protein degradation of H2B (Figures 1B and S2), the K120R mutant also showed an increased resistance to the nucleoli-mediated protein degradation *in vitro* compared with that of wild-type H2B (Figure 5C). Although the H2BK120R mutant is more stable than wild-type H2B, the H2BK120R mutant was still degraded ultimately (Figure 5C), suggesting that additional lysine residues may also be ubiquitinated and involved in the protein degradation in the *in vitro* system. More interestingly, the addition of the proteasome inhibitor MG132 to the *in vitro* reaction system completely abolished the protein degradation of the purified GST-H2B, suggesting that the nucleolus-mediated H2B protein degradation is achieved through the proteasome pathway (Figure 5D). Furthermore, incubation with the nucleolus fractions also resulted in the ubiquitination of the purified GST-H2B (Figure 5E), whereas the cytoplasm and nucleoplasm fractions did not show similar effects (Figure 5G). Thus, our *in vitro* experiments indicated that the nucleolus fractions likely contain essential components that are required for H2B ubiquitination and degradation, therefore strongly supporting the conclusion that histone H2B is degraded through a nucleolus-related pathway. In addition, our immunofluorescence analysis and nucleolus isolation followed by western blot analysis also supported this notion, as we found that two proteasome subunits, PSMD1 (a non-ATPase subunit of proteasome) and ADRM1 (act as an ubiquitin receptor in proteasome), were colocalized with NCL (Figures S7A and S7B, both proteins were whole-cell distributed and showed fluorescence signals at the nucleolus compartment) and existed in the nucleolus extracts (Figure S7C), suggesting that nucleolus may contain proteasomes. Moreover, our 4D label-free proteomic analysis for the nucleolus extracts also supported the above speculation, as multiple proteasome components and protein ubiquitination-related enzymes were identified (Table S1). In addition, the original proteomic data were also uploaded to the public repository ProteomeXchange via the PRIDE database. The accession number is "ProteomeXchange: PXD023415."

Moreover, general chase experiment (Figure 6A, left) and the SNAP-tag-based chase experiment (Figure 6A, right, and Figure S8) were performed respectively in both nucleolus fraction and non-nucleolus fraction to determine the degradation rate of H2B in these two compartments *in vivo*. Of great interest, we found that H2B in the nucleolus fraction degraded much faster than that in the non-nucleolus fraction (Figures 6A and S8), further supporting our speculation that H2B is likely degraded in the nucleolus.

We accidentally found that the H2B protein levels were strikingly higher in mouse testis than in other tissues (Figure S9A, left). To determine whether the observed higher levels of H2B protein in the testis are due to elevated mRNA levels, the mRNA levels of H2B in multiple tissues were examined. However, no obvious

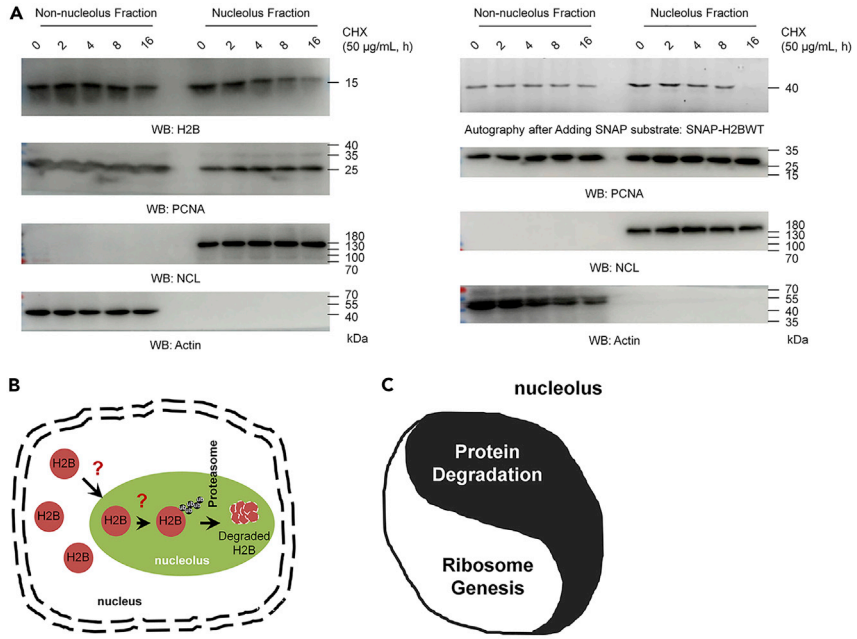

Figure 6. The degradation rate of H2B in the nucleolus fractions and non-nucleolus fractions, and working model

(A) 293T cells were treated with 50 μg/mL cycloheximide (CHX) for the indicated time points. The nucleolus fractions and non-nucleolus fractions were prepared respectively. Western blot analysis with antibodies as indicated was performed (left). 293T cells were transfected with a SNAP-tagged wild-type H2B (SNAP-H2BWT) plasmid for 48 h, and cells were then treated with 50 μg/mL CHX for the indicated time points. The nucleolus fractions and non-nucleolus fractions were prepared respectively. Autography analysis by adding SNAP substrate and western blot analysis with antibodies as indicated was performed (right).

(B) H2B is degraded through a nucleolus-mediated pathway in a ubiquitination-proteasome-dependent manner.

(C) The nucleolus likely plays a "yin-yang"-like role in the control of protein dosage.

increase in H2B mRNA levels in the testis was observed (Figure S9A, right), suggesting that a posttranscriptional mechanism (such as an impaired protein degradation activity) may be involved in the observed higher levels of H2B protein in the testis. More interestingly, although histone H3 is also a core histone, in contrast to H2B, histone H3 did not show obvious changes between different tissues (Figure S9A, left), suggesting that, in addition to the canonical structural functions in chromatin assembly, H2B may possess other regulatory roles that are still unknown. This notion was also supported by a recent study that the expression of multiple H2B isoforms was increased in different types of lung cancers, and high H2B levels predicted low survival in all types of lung cancer patients. They therefore suspected that H2B could be a biomarker for determining the prognosis of lung cancer (Zeng et al., 2020). Furthermore, we also examined the distribution of H2B in multiple tissues. Intriguingly, we found that, in parallel with the findings of higher H2B protein levels in testis, the nucleolus in testis showed a nontypical pattern (increased number, fragmented shape, and dispersed signals in the non-nucleolus nuclear area) (Figure S9B), suggesting that noncanonical nucleoli may exist in the testis, which may contribute to the accumulation of H2B protein in testis. Moreover, the H2B signals also did not co-stain with the nucleolus marker (NCL) signals (Figure S9B), suggesting that the irregular nucleolus may also abolish the stable residence of H2B in the nucleolus and further impair the degradation of H2B. More interestingly, some of the H2B staining in other tissues showed a relatively higher signal surrounding the nucleolus forming a ring-like pattern (Figure S9B), supporting the idea that the portion of H2B in the nucleolus may be normally degraded.

DISCUSSION

Eukaryotic histones are the major components that package DNA into chromatin, and the amount of histones is crucial for the organization and stability of higher order chromatin structures (Margueron and Reinberg, 2010; Venkatesh and Workman, 2015). However, the mechanisms regulating the amount of histones are understudied, and more importantly, the molecular mechanisms of how histones are degraded are

especially poorly understood. In this study, we demonstrated that a novel nucleolus-related pathway may participate in the regulation of histone H2B degradation in a ubiquitination-proteasome activity-dependent manner (Figure 6B). Our data indicated that the protein degradation of H2B is mainly achieved through the ubiquitination-proteasome pathway, as only the proteasome inhibitor MG132 treatment could result in the accumulation of H2B (Figures 1A, 1D, and S4B). Moreover, the K120 site of H2B was essential for its protein degradation (Figures 2B–2D and S2), and in parallel with the defect in protein degradation of K120R-mutated H2B, a significant decrease in the polyubiquitination of K120R-mutated H2B was also observed (Figures 2E–2G). Importantly, when cells were treated with MG132, more H2B accumulated in the nucleolus, similar to the distribution of degradation-defective K120R-mutated H2B (Figures 4A–4D and 3A–3C). The accumulation of H2B in the nucleolus under MG132 treatment is likely due to the blockage of H2B degradation, rather than a rearrangement of H2B distribution, as no other fractions showed changes in H2B protein levels except the nucleolus fraction (Figures 4C and 4D). Most importantly, our *in vitro* studies strongly supported that the nucleolus is likely the compartment that is essential for H2B protein ubiquitination and degradation (Figure 5). Therefore, these findings elucidate a previously unknown mechanism by which the nucleolus mediates the protein degradation of histone H2B.

Recently, increasing studies have indicated that, in addition to the canonical functions of regulating ribosome biogenesis, the nucleolus also plays significant roles in protein quality control (Frottin et al., 2019; Amer-Sarsour and Ashkenazi, 2019; Azkanaz et al., 2019; Rekulapally and Suresh, 2019) and degradation (Song and Wu, 2005; Tao et al., 2013; Guan et al., 2016). For instance, Survivin-deltaEx3, a splice variant of Survivin, was reported to be degraded through the nucleolus-mediated protein degradation pathway in a ubiquitination-proteasome-dependent manner (Song and Wu, 2005). In addition, the degradation of p53 was also reported to be regulated by the nucleolus-related protein degradation pathway. Def, a nucleolar protein, mediates the degradation of p53 protein in the nucleolus. In contrast to both Suvivin-deltaEX3 and H2B, Def-mediated nucleolar degradation of p53 is independent of the proteasome pathway but is dependent on the activity of Calpain3, a cysteine protease (Tao et al., 2013; Guan et al., 2016). Although we failed to identify the specific regulators regulating the nucleolar transport of unnecessary H2B and enzymes catalyzing nucleolus-related H2B degradation, our results further highlighted the critical roles of the nucleolus in the control of protein degradation, especially in regulating histone degradation. However, further studies are needed to identify the related enzymes and regulatory factors involved in nucleolus-mediated H2B degradation. Therefore, together with the canonical roles in the regulation of ribosome genesis and protein translation of the nucleolus, we revealed a "yin-yang"-like regulatory function of the nucleolus in the control of protein dosage (Figure 6C).

Limitations of the study

This study revealed a novel role of the nucleolus that likely functions as the compartment for histone H2B protein degradation and also suggested a previously unappreciated mechanism in the regulation of histone H2B protein degradation. However, as we discussed, the specific regulators regulating the nucleolar transport of unnecessary H2B and enzymes catalyzing nucleolus-related H2B degradation have not been identified in the current study. Therefore, we will pay more efforts in the future.

Resource availability

Lead contact

Further information and requests for resources and reagents should be directed to and will be fulfilled by the lead contact, Dr. Su Chen (chensu@xjtu.edu.cn).

Materials availability

Materials used or generated in this study will be available upon reasonable request, and a material transfer agreement may be required.

Data and code availability

The accession number for the 4D label-free proteomic data reported in this paper is "ProteomeXchange: PXD023415".

METHODS

All methods can be found in the accompanying transparent methods supplemental file.

SUPPLEMENTAL INFORMATION

Supplemental information can be found online at https://doi.org/10.1016/j.isci.2021.102256.

ACKNOWLEDGMENTS

This work was supported by the National Natural Science Foundation of China (Grant No.: 81773009, 81972650), the China Postdoctoral Science Foundation (Grant No.: 2017M613149 and 2018T111038), and the Fundamental Research Funds for the Central Universities (Xi'an Jiao Tong University, Grant No.: 2017qngz13).

AUTHOR CONTRIBUTIONS

SC designed the study; YL, YW, LY, FS, SL, YQW, GAZ, TD, LLZ, WD, XZ, and WC performed the experiments; SC and LY analyzed the data; SC wrote the manuscript.

DECLARATION OF INTERESTS

The authors declare that they have no competing interests.

Received: April 29, 2020
Revised: February 4, 2021
Accepted: February 25, 2021
Published: April 23, 2021

REFERENCES

Amer-Sarsour, F., and Ashkenazi, A. (2019). The nucleolus as a proteostasis regulator. Trends Cell Biol. *29*, 849–851.

Azkanaz, M., Rodríguez López, A., de Boer, B., Huiting, W., Angrand, P.O., Vellenga, E., Kampinga, H.H., Bergink, S., Martens, J.H., Schuringa, J.J., and van den Boom, V. (2019). Protein quality control in the Nucleolus safeguards recovery of epigenetic regulators after heat shock. Elife *8*, pii: e45205.

Bassermann, F., Eichner, R., and Pagano, M. (2014). The ubiquitin proteasome system-implications for cell cycle control and the targeted treatment of cancer. Biochim. Biophys. Acta *1843*, 150–162.

Behrends, C., and Harper, J.W. (2011). Constructing and decoding unconventional ubiquitin chains. Nat. Struct. Mol. Biol. *18*, 520–528.

Cao, J., and Yan, Q. (2012). Histone ubiquitination and deubiquitination in transcription, DNA damage response, and cancer. Front. Oncol. *2*, 26.

Chan, J.C., and Maze, I. (2020). Nothing is yet set in (Hi)stone: novel post-translational modifications regulating chromatin function. Trends Biochem. Sci. *45*, 829–844.

Chen, Y.S., and Qiu, X.B. (2012). Transcription-coupled replacement of histones: degradation or recycling? J. Genet. Genomics *39*, 575–580.

Chi, P., Allis, C.D., and Wang, G.G. (2010). Covalent histone modifications–miswritten, misinterpreted and mis-erased in human cancers. Nat. Rev. Cancer *10*, 457–469.

Clague, M.J., and Urbé, S. (2010). Ubiquitin: same molecule, different degradation pathways. Cell *143*, 682–685.

Deal, R.B., Henikoff, J.G., and Henikoff, S. (2010). Genome-wide kinetics of nucleosome turnover determined by metabolic labeling of histones. Science *328*, 1161–1164.

Dion, M.F., Kaplan, T., Kim, M., Buratowski, S., Friedman, N., and Rando, O.J. (2007). Dynamics of replication-independent histone turnover in budding yeast. Science *315*, 1405–1408.

Frottin, F., Schueder, F., Tiwary, S., Gupta, R., Körner, R., Schlichthaerle, T., Cox, J., Jungmann, R., Hartl, F.U., and Hipp, M.S. (2019). The nucleolus functions as a phase-separated protein quality control compartment. Science *365*, 342–347.

Guan, Y., Huang, D., Chen, F., Gao, C., Tao, T., Shi, H., Zhao, S., Liao, Z., Lo, L.J., Wang, Y., et al. (2016). Phosphorylation of Def regulates nucleolar p53 turnover and cell cycle progression through Def recruitment of Calpain3. PLoS Biol. *14*, e1002555.

Hammoud, S.S., Nix, D.A., Zhang, H., Purwar, J., Carrell, D.T., and Cairns, B.R. (2009). Distinctive chromatin in human sperm packages genes for embryo development. Nature *460*, 473–478.

Hauer, M.H., Seeber, A., Singh, V., Thierry, R., Sack, R., Amitai, A., Kryzhanovska, M., Eglinger, J., Holcman, D., Owen-Hughes, T., and Gasser, S.M. (2017). Histone degradation in response to DNA damage enhances chromatin dynamics and recombination rates. Nat. Struct. Mol. Biol. *24*, 99–107.

Huang, H., Sabari, B.R., Garcia, B.A., Allis, C.D., and Zhao, Y. (2014). SnapShot: histone modifications. Cell *159*, 458.

Kim, J., Hake, S.B., and Roeder, R.G. (2005). The human homolog of yeast BRE1 functions as a transcriptional coactivator through direct activator interactions. Mol. Cell *20*, 759–770.

Li, Z.F., and Lam, Y.W. (2015). A new rapid method for isolating nucleoli. Methods Mol. Biol. *1228*, 35–42.

Liang, Y.M., Wang, X., Ramalingam, R., So, K.Y., Lam, Y.W., and Li, Z.F. (2012). Novel nucleolar isolation method reveals rapid response of human nucleolar proteomes to serum stimulation. J. Proteomics *77*, 521–530.

Lu, Z., and Hunter, T. (2009). Degradation of activated protein kinases by ubiquitination. Annu. Rev. Biochem. *78*, 435–475.

Luger, K., Mäder, A.W., Richmond, R.K., Sargent, D.F., and Richmond, T.J. (1997). Crystal structure of the nucleosome core particle at 2.8 A resolution. Nature *389*, 251–260.

Margueron, R., and Reinberg, D. (2010). Chromatin structure and the inheritance of epigenetic information. Nat. Rev. Genet. *11*, 285–296.

Mills, N.C., Van, N.T., and Means, A.R. (1977). Histones of rat testis chromatin during early postnatal development and their interactions with DNA. Biol. Reprod. *17*, 760–768.

Rekulapally, P., and Suresh, S.N. (2019). Nucleolus: a protein quality control compartment. Trends Biochem. Sci. *44*, 993–995.

Song, Z., and Wu, M. (2005). Identification of a novel nucleolar localization signal and a degradation signal in Survivin-deltaEx3: a potential link between nucleolus and protein degradation. Oncogene *24*, 2723–2734.

Strahl, B.D., and Allis, C.D. (2000). The language of covalent histone modifications. Nature *403*, 41–45.

Tao, T., Shi, H., Guan, Y., Huang, D., Chen, Y., Lane, D.P., Chen, J., and Peng, J. (2013). Def

defines a conserved nucleolar pathway that leads p53 to proteasome-independent degradation. Cell Res. *23*, 620–634.

Venkatesh, S., and Workman, J.L. (2015). Histone exchange, chromatin structure and the regulation of transcription. Nat. Rev. Mol. Cell Biol. *16*, 178–189.

Weake, V.M., and Workman, J.L. (2008). Histone ubiquitination: triggering gene activity. Mol. Cell *29*, 653–663.

Wu, J., Huen, M.S., Lu, L.Y., Ye, L., Dou, Y., Ljungman, M., Chen, J., and Yu, X. (2009). Histone ubiquitination associates with BRCA1-dependent DNA damage response. Mol. Cell Biol. *29*, 849–860.

Xia, Y., Yang, W., Fa, M., Li, X., Wang, Y., Jiang, Y., Zheng, Y., Lee, J.H., Li, J., and Lu, Z. (2017). RNF8 mediates histoneH3 ubiquitylation and promotes glycolysis and tumorigenesis. J. Exp. Med. *214*, 1843–1855.

Zeng, Z., Lu, J., Wu, D., Zuo, R., Li, Y., Huang, H., Yuan, J., and Hu, Z. (2020). Poly(ADP-ribose) glycohydrolase silencing-mediated H2B expression inhibits benzo(a)pyrene-induced carcinogenesis. Environ. Toxicol. *36*, 291–297, https://doi.org/10.1002/tox.23034.

Zhang, Y. (2003). Transcriptional regulation by histone ubiquitination and deubiquitination. Genes Dev. *17*, 2733–2740.

Zhu, B., Zheng, Y., Pham, A.D., Mandal, S.S., Erdjument-Bromage, H., Tempst, P., and Reinberg, D. (2005). Monoubiquitination of human histone H2B: the factors involved and their roles in HOX gene regulation. Mol. Cell *20*, 601–611.

iScience, Volume *24*

Supplemental information

The nucleolus functions as the compartment for histone H2B protein degradation

Yanping Liu, Yufei Wang, Lu Yang, Feng Sun, Sheng Li, Yequan Wang, Guo-An Zhang, Tingting Dong, Lei-Lei Zhang, Wanglin Duan, Xiaojun Zhang, Wen Cui, and Su Chen

Supplemental Information

Supplemental Figures and Figure Legends

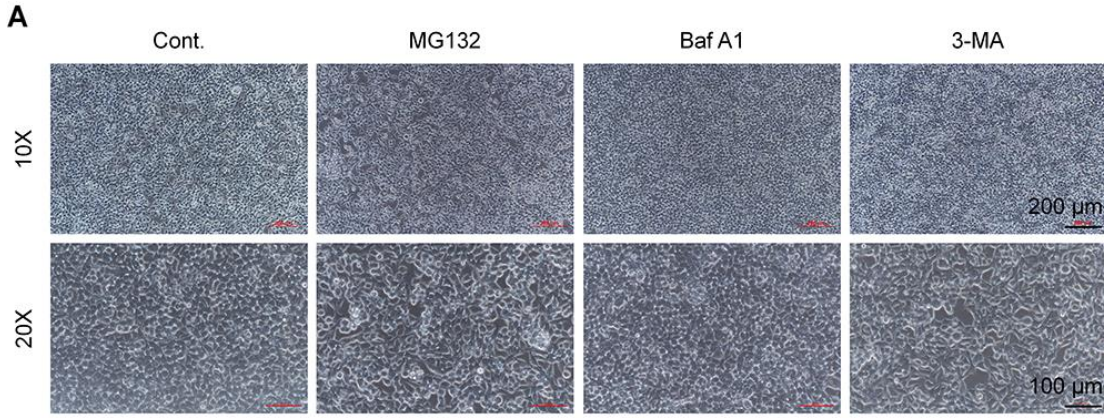

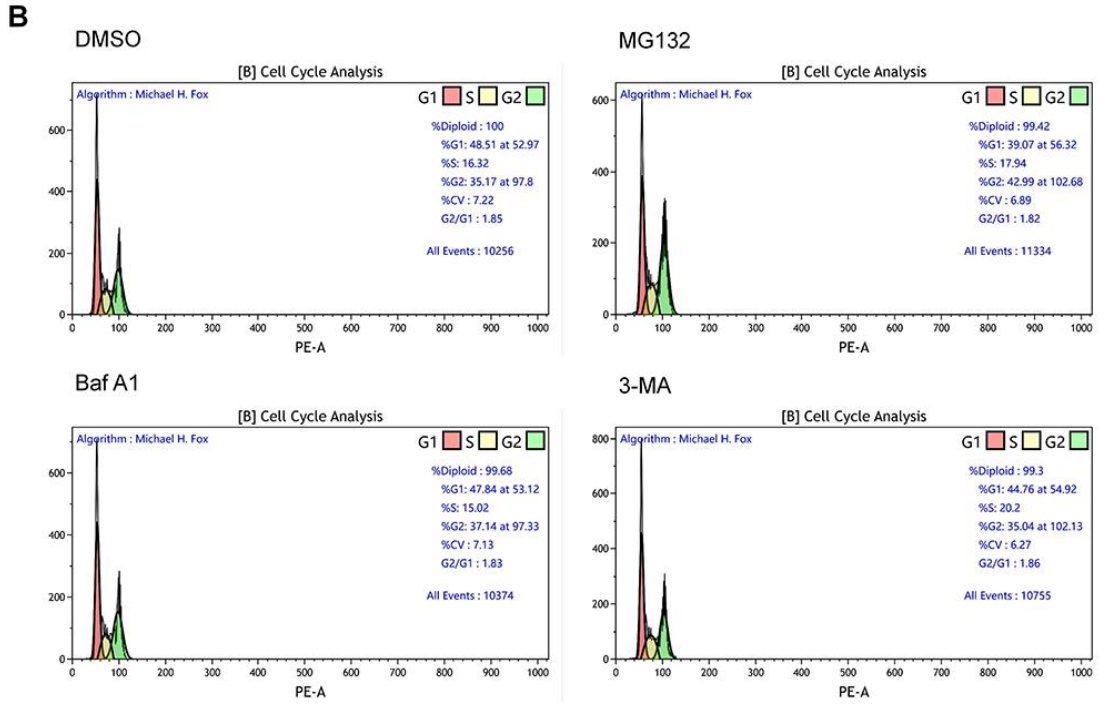

	DMSO	MG132	Baf A1	3-MA
% of G1	48.51	39.07	47.84	44.76
% of S	16.32	17.94	15.02	20.2
% of G2/M	35.17	42.99	37.14	35.04

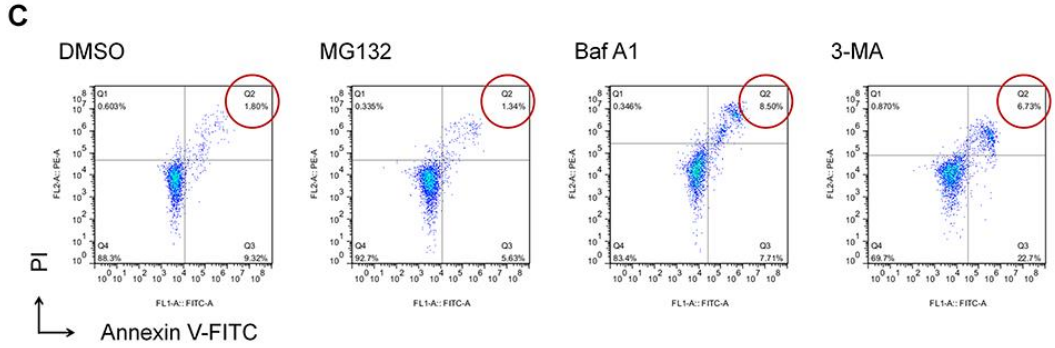

	DMSO	MG132	Baf A1	3-MA
% of Apoptosis	1.8%	1.34%	8.50%	6.73%

Figure S1. The effects of protein degradation inhibitors used in this study (Baf A1, 3-MA, and MG132) on cell cycle and apoptosis. Related to Figure 1.

A, 293T cells were treated with DMSO, MG132 (25 μM), Baf A1 (0.5 μM), and 3-MA (10 mM) for 10 h. Cells were then photographed with an optical microscopy.

B, 293T cells were treated with DMSO, MG132 (25 μM), Baf A1 (0.5 μM), and 3-MA (10 mM) for 10 h. Cells were then stained with PI (Propidium Iodide) and subjected to cell cycle analysis under the instruction of the Cell Cycle Analysis Kit (#C1052, Beyotime, China).

C, 293T cells were treated with DMSO, MG132 (25 μM), Baf A1 (0.5 μM), and 3-MA (10 mM) for 10 h. Cells were then stained with PI and FITC-labeled Annexin V and subjected to cell apoptosis analysis under the instruction of the Cell Apoptosis Detection Kit (#C1062, Beyotime, China). The PI and Annexin V-FITC double positive cells are recognized as the apoptotic cells.

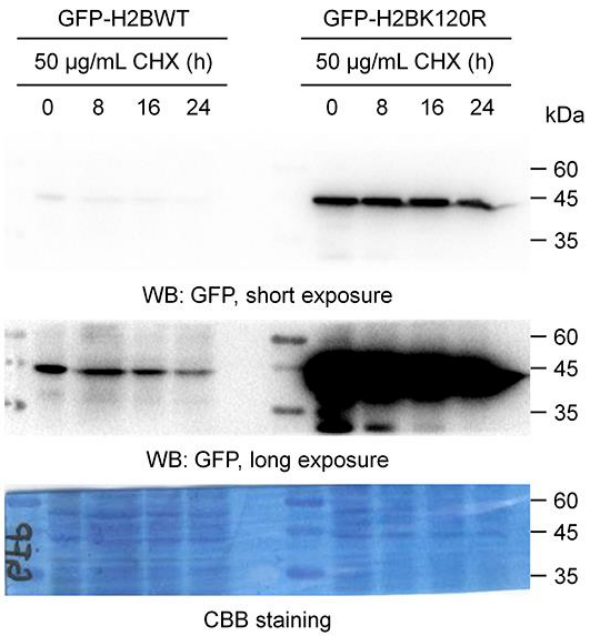

Figure S2. Mutation of lysine 120 to arginine (K120R) in H2B impaired the protein degradation of H2B. Related to Figure 1.

Western blot analysis of 293T cells transfected with a GFP-H2BWT or a GFP-H2BK120R plasmid, and treated with CHX for the indicated time points.

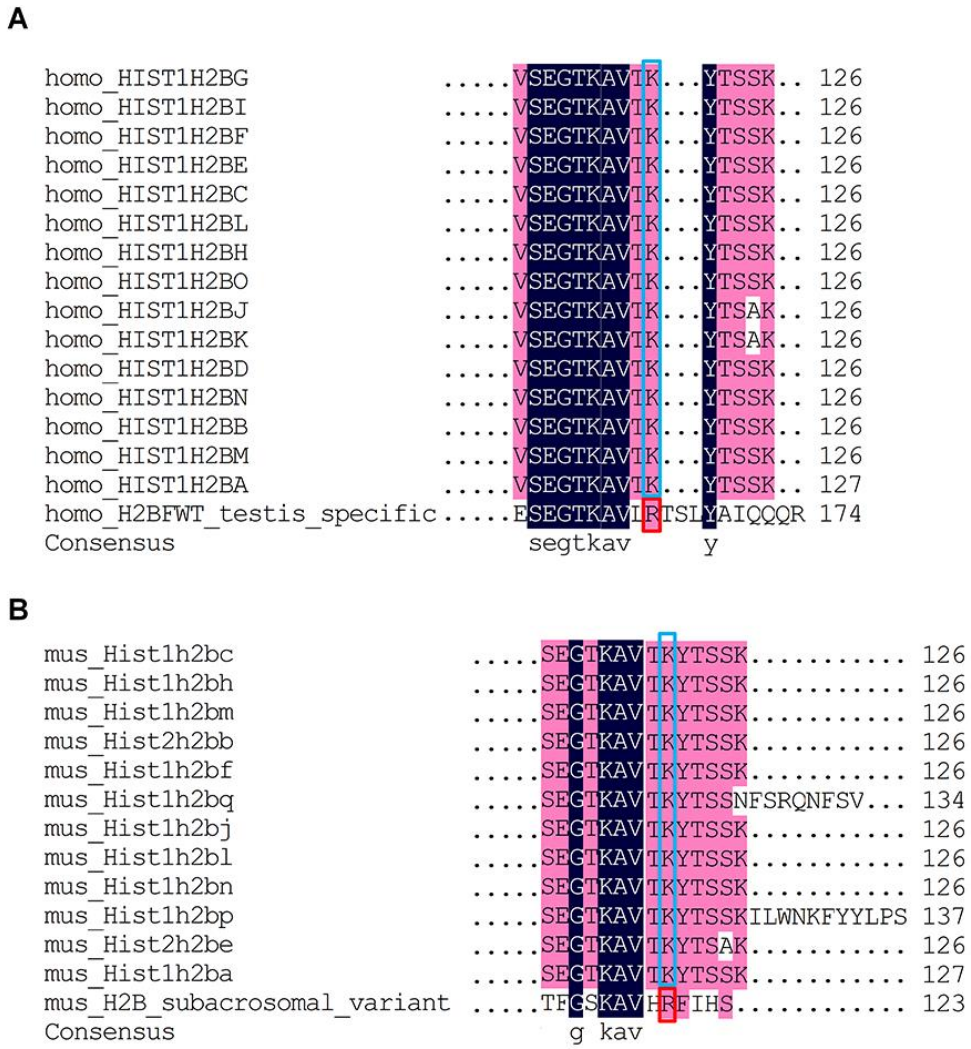

Figure S3. Alignment of distinct isoforms of human and mouse H2B. Related to Figure 2 and Figure 3.

A and B, Alignment of distinct isoforms of human (A) and mouse (B) H2B.

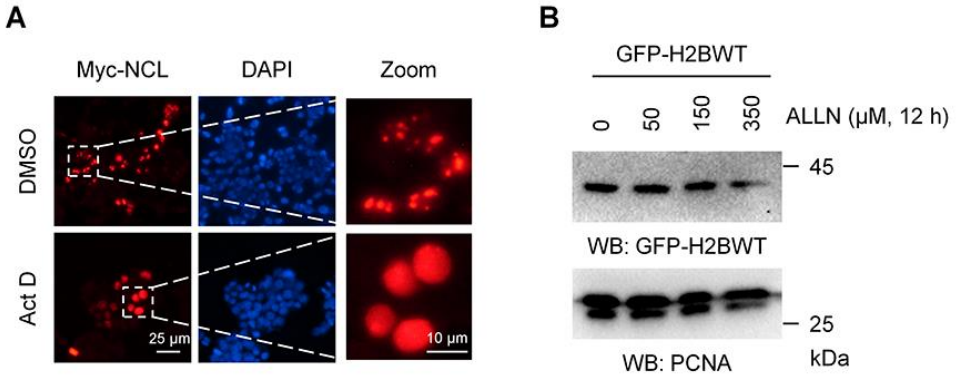

Figure S4. The effect of Act D on the distribution of NCL, and the effect of ALLN on the protein levels of H2B. Related to Figure 4.

A, Myc-NCL transfected 293T cells were further treated with 100 ng/ml Act D for 10 h. Cells were then subjected to immunofluorescence analysis with Myc-tag antibodies.

B, Western blot analysis of 293T cells treated with an increased dosage of the calpain inhibitor ALLN for 12 h.

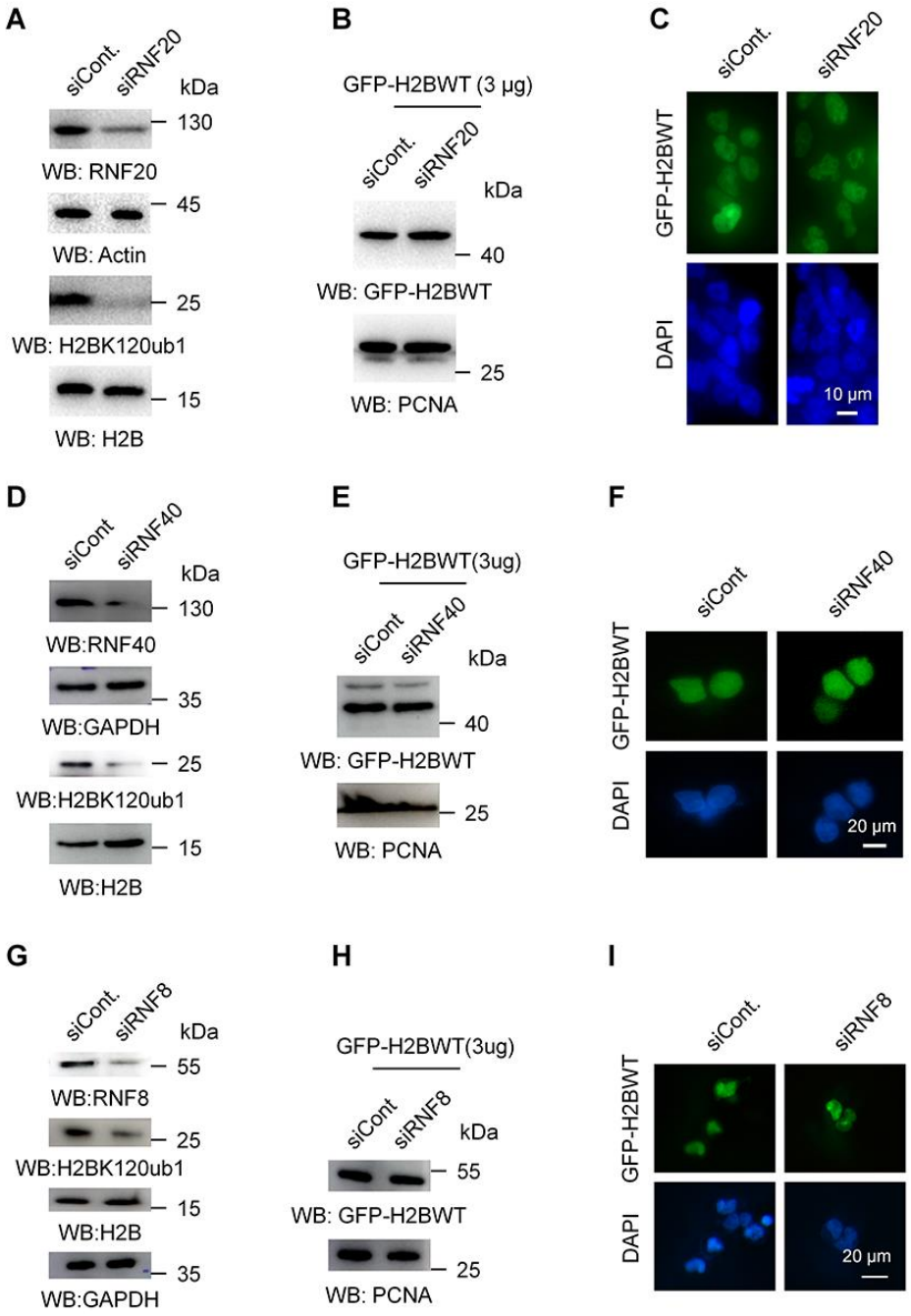

Figure S5. H2B monoubiquitination-related enzymes, RNF20, RNF40, and RNF8, did not affect the protein levels and localization of H2B. Related to Figure 4.

A, D, and G, 293T cells were transfected with RNF20-, RNF40-, and RNF8-specific siRNAs as indicated for 48 h. Cells were then harvested and subjected to Western blot analyses to determine the knockdown efficiencies of the siRNAs.

B, E, and H, 293T cells were transfected with RNF20-, RNF40-, and RNF8-specific siRNAs as indicated

together with a GFP-tagged wild-type H2B construct (GFP-H2BWT) for 48 h. Cells were then harvested and subjected to Western blot analyses to determine the effects of RNF20, RNF40, and RNF8 on H2B protein levels.

C, F, and I, 293T cells were transfected with RNF20-, RNF40-, and RNF8-specific siRNAs as indicated together with a GFP-tagged wild-type H2B construct (GFP-H2BWT) for 48 h. Cells were then subjected to fluorescence microscopy analyses to determine the effects of RNF20, RNF40, and RNF8 on H2B localization.

The siRNAs were all purchased from Santa Cruz Biotechnology (#sc-92753 for RNF20, #sc-93054 for RNF40, and #sc-61484 for RNF8).

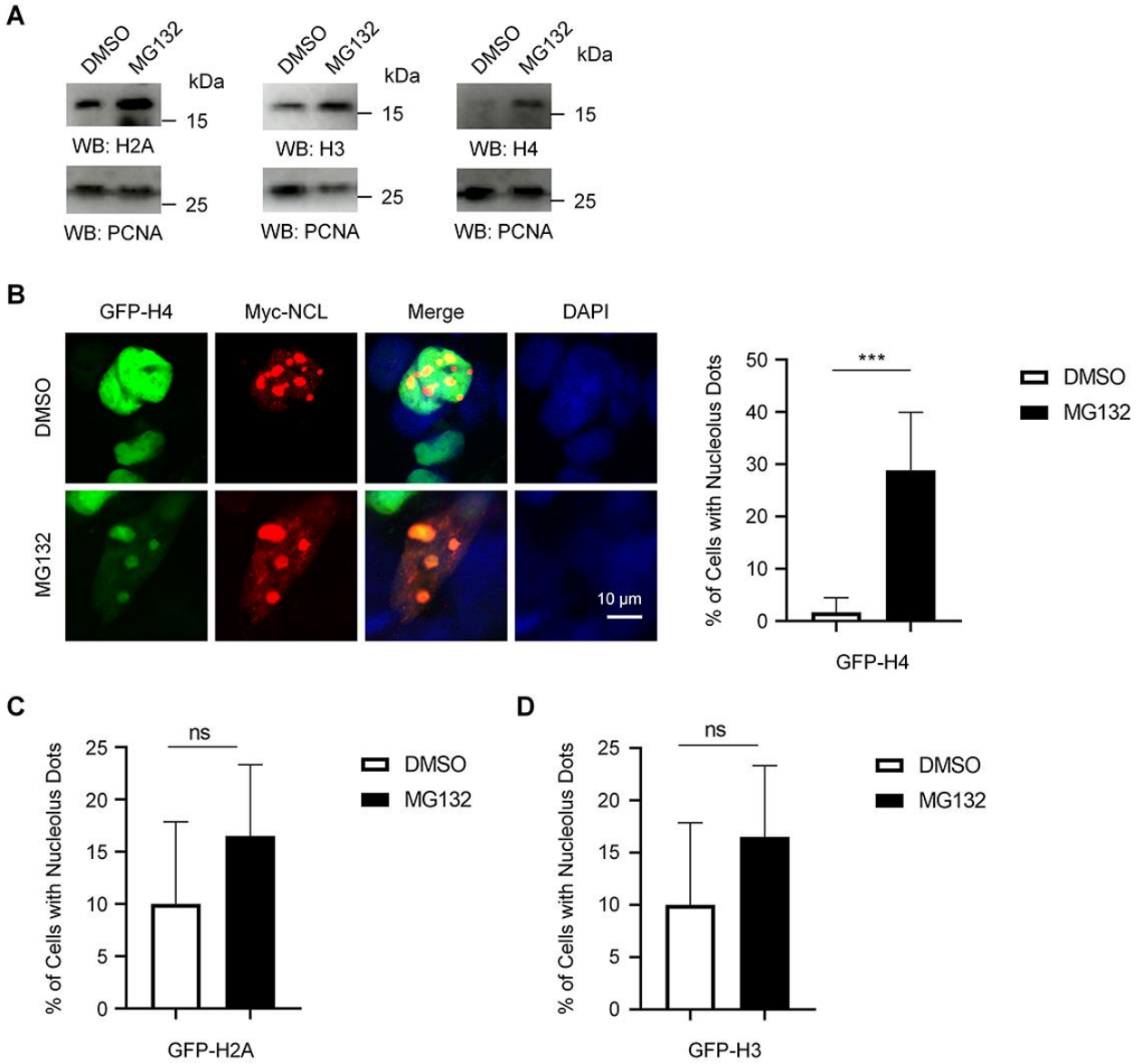

Figure S6. The effect of MG132 on the localization of H2A, H3, and H4. Related to Figure 4.

A, Western blot analyses in 293T cells treated with 25μM MG132 for 10 h or with DMSO as a negative

control.

B, GFP-tagged H4 transfected 293T cells were further treated with 25μM MG132 for 10 h. Cells were then subjected to immunofluorescence analysis. The percentage of cells with H4 dots in the nucleolus was calculated (right). More than 500 cells were counted in each group.

C, GFP-tagged H2A transfected 293T cells were further treated with 25μM MG132 for 10 h. Cells were then subjected to immunofluorescence analysis. The percentage of cells with H2A dots in the nucleolus was calculated. More than 500 cells were counted in each group.

D, GFP-tagged H3 transfected 293T cells were further treated with 25μM MG132 for 10 h. Cells were then subjected to immunofluorescence analysis. The percentage of cells with H3 dots in the nucleolus was calculated. More than 500 cells were counted in each group.

All the experiments were repeated more than 3 times, similar results were obtained, and representative images were provided. Bars and error bars are the mean ± s.d., n=3 independent repeats. Two-tailed unpaired Student's t-test was performed. ***: $P<0.001$, ns: no significance.

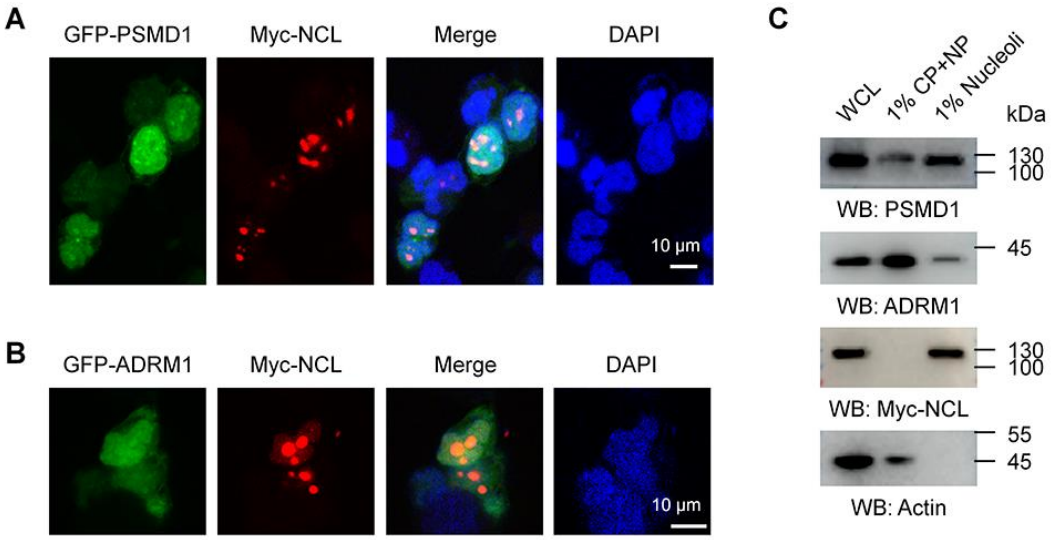

Figure S7. Two proteasome components, ADRM1 and PSMD1, were distributed in the nucleolus. Related to Figure 4 and Figure 5.

A, 293T cells were transfected with a GFP-tagged PSMD1 construct together with a Myc-tagged NCL construct for 48 h. Cells were then subjected to immunofluorescence analysis.

B, 293T cells were transfected with a GFP-tagged ADRM1 construct together with a Myc-tagged NCL construct for 48 h. Cells were then subjected to immunofluorescence analysis.

C, Nucleolus isolation followed by Western blot analysis was performed in 293T cells transfected with a a Myc-NCL plasmid.

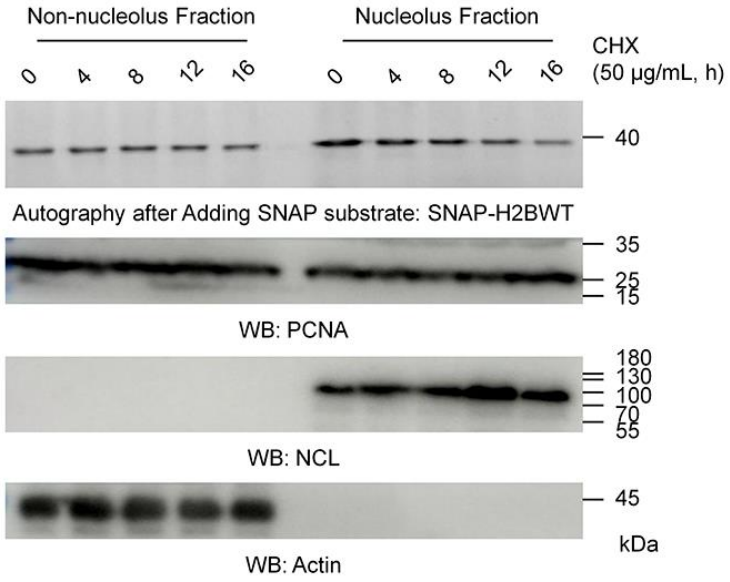

Figure S8. The degradation rate of H2B in the nucleolus fractions and non-nucleolus fractions. Related to Figure 6.

293T cells were transfected with a SNAP-tagged wild type H2B (SNAP-H2BWT) plasmid for 48 h, and cells were then treated with 50 μg/ml CHX for the indicated time points. The nucleolus fractions and non-nucleolus fractions were prepared respectively. Autography analysis by adding SNAP substrate and Western blot analysis with antibodies as indicated were performed.

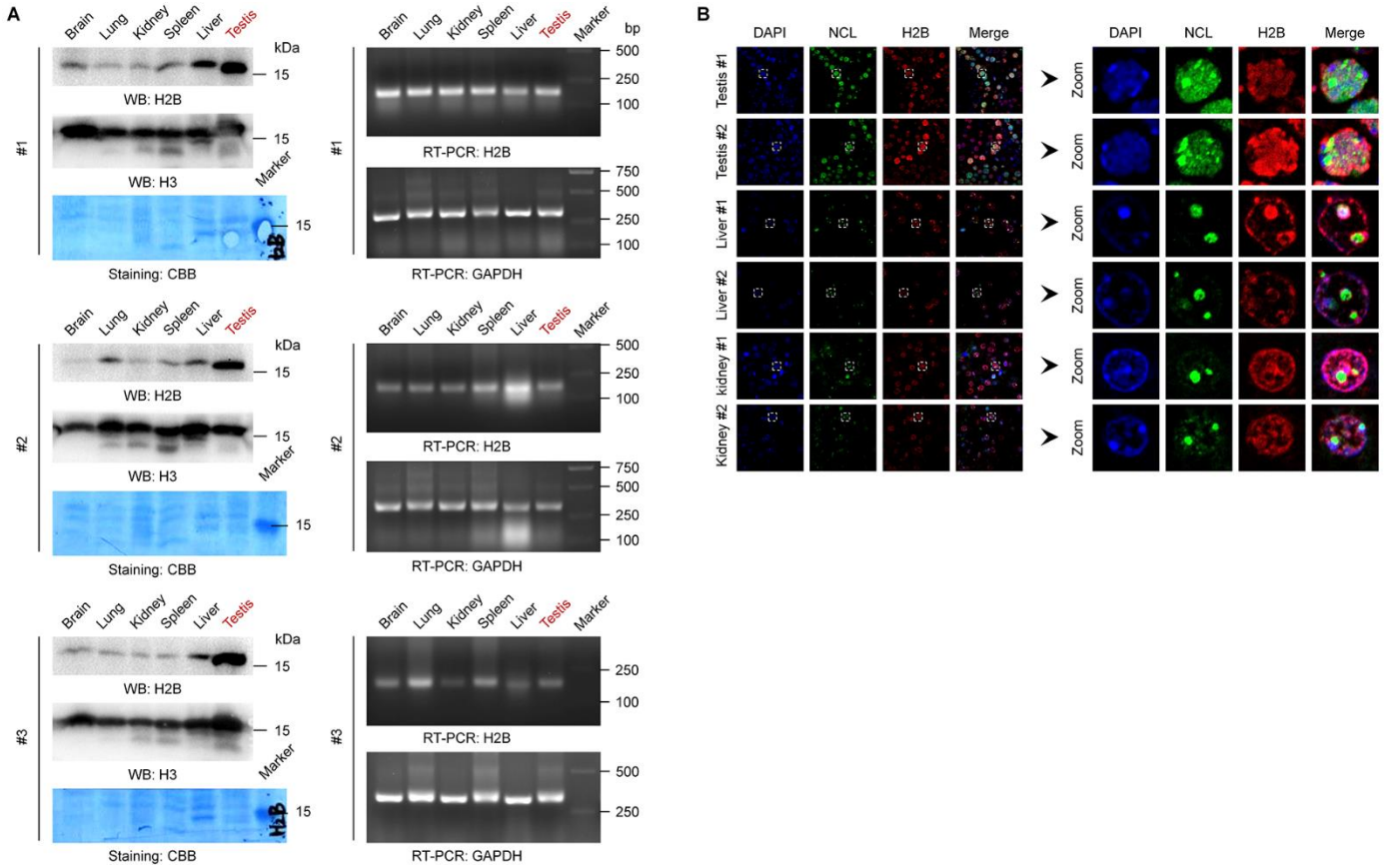

Figure S9. H2B protein levels are higher in testis than in other tissues. Related to Figure 3-Figure 6.

A, Western blot (left) and RT-PCR (right) assays of H2B protein levels in multiple mouse tissues.

B, IF assays of H2B in multiple mouse tissues.

Supplemental Tables

Table S2. Primers used in the RT-PCR analyses. Related to Figure 1, Figure 2, and Figure S9.

GFP	Forward: 5'-TATCATGGCCGACAAGCAGA-3'
	Reverse: 5'-ATGTGATCGCGCTTCTCGTT-3'
GAPDH (Homo)	Forward: 5'-GACAGTCAGCCGCATCTTCT-3'
	Reverse: 5'-AAATGAGCCCCAGCCTTCTC-3'
H2B (Mus)	Forward: 5'-AAGGCGCAGAAGAAGGATGG-3'
	Reverse: 5'-CGATGCGCTCGAAGATGTC-3'
GAPDH (Mus)	Forward: 5'- CCTGCACCACCAACTGCTTA-3'
	Reverse: 5'- TACTTGGCAGGTTTCTCCAGG-3'

Transparent Methods

Cell culture and transfection

The human embryonic kidney cell line HEK-293T was cultured in DMEM (high glucose, HyClone, #SH30022.01) supplemented with 10% fetal bovine serum and 1% penicillin and streptomycin in a humidified 5% CO_2 atmosphere at 37 ℃. Transfection of cells was performed by using Lipofectamine 2000 (Invitrogen, #11668-019) according to the manufacturer's standard protocol.

Plasmid construction

All cDNAs of human H2BWT, H2BK120R, H2BFWT, H2BFWTR164K, and nucleolin were amplified by RT-PCR from total RNA extracted from 293T cells. PCR-amplified human H2BWT, H2BK120R, H2BFWT, H2BFWTR164K cDNAs were inserted into the pEGFP-N1 vector, and nucleolin was cloned into the pCMV-Myc vector. SNAP-H2BWT was constructed with the H2BWT cDNA and the pSNAPf vector. Recombinant plasmids of pET-42b (+) encoding GST-tagged H2BWT and H2BK120R were also constructed with the cDNAs of H2BWT and H2BK120R.

Protein ubiquitination analysis (under denaturing conditions)

Cells were transfected with the indicated constructs using Lipofectamine 2000 (Invitrogen, #11668-019) for 48 h. To detect H2B ubiquitylation *in vivo*, the cells were harvested and washed with ice-cold PBS for three times. Cells were lysed in 100 μl ATM lysis buffer containing 1% SDS (100 mM Tris-Cl, pH 7.5; 150 mM NaCl; 0.2 mM EDTA; 20% glycerol; 0.4% NP-40; 2% Tween-20; 1% SDS; 1 mM DTT; and 0.2 mM PMSF) for 30 min on ice, and boiled for 10 min, and then another 900 μl ATM lysis buffer without SDS (100 mM Tris-Cl, pH 7.5; 150 mM NaCl; 0.2 mM EDTA; 20% glycerol; 0.4% NP-40; 2% Tween-20; and 0.2 mM PMSF) was added to dilute the SDS concentration. The lysed cells were subjected to sonication on ice for 10 times (3 s each) with 20% efficiency. Cell lysates were incubated with normal IgG (as a negative control, Santa Cruz Biotechnology, #sc-2025) or the indicated antibodies for immunoprecipitation at 4 ℃ overnight. Protein A/G agarose beads (Santa Cruz Biotechnology, #sc-2003) were subsequently added and incubated for another 3 h. The solution was centrifuged to harvest the agarose beads after they were washed 5 times with lysis buffer. The precipitated proteins were released by boiling in loading buffer and resolved via SDS–PAGE. Western blot analyses were performed with related antibodies.

Antibodies and Western blot analysis

The antibodies against H3 (#4499), H2B (#12364), K48-linkage specific polyubiquitin (#4289), K63-linkage specific polyubiquitin (#5621) and LC3B (#2775) were purchased from Cell Signaling Technology. The antibodies against Myc tag (#M20002), GFP tag (#P30010), and Actin (#M20011) were purchased from Abmart (Shanghai, China). The antibodies against PCNA (#A13336) and GST (#AE006) were purchased from ABclonal. The antibody against ubiquitin (#ab7780) was purchased from Abcam.

Cells were harvested after treatment, rinsed in ice-cold PBS, and lysed in ATM lysis buffer on ice for 30 min. The lysates were centrifuged at 12000 rpm for 10 min at 4 ℃ to remove any cellular debris, and boiled for 10 min. The protein concentration of the lysates was determined by a BCA assay (#CW0014, CWBIO, China). Next, samples were loaded into a 10% or 15% gel to resolve the proteins, transferred to PVDF membranes (Amersham, #10600021), and blocked with 5% nonfat dry milk in PBS-Tween-20 (0.1%) for 3 h at room temperature. The membrane was incubated with primary antibodies overnight. After washing, the membrane was incubated with the appropriate HRP-labeled secondary antibodies (diluted 1:4000; Zhongshan Golden Bridge, #ZDR-5306 or #ZDR-5307) for 2 h. Following several washes, the signals on the membrane were detected by an eECL Western blot kit (#CW0049M, CWBIO, China).

RT-PCR assay

Cells were lysed to isolate total RNA using TRIzol reagent (#15596026, Thermo) according to the manufacturer's instructions. Reverse transcription was performed using a Reverse Transcription Kit (#6110A, Takara). Briefly, total RNA (5 μg) was reverse transcribed to synthesize cDNA in a reaction volume of 20 μl using MMLV reverse transcriptase. In each 25 μl PCR mixture, 1 μl of cDNA was used for RT-PCR analyses. PCR products were loaded onto a 2% agarose gel, stained with ethidium bromide, and imaged. The sequences of the primers used in this study are listed in **Table S2**.

Immunofluorescence (IF) analysis

Cells transfected with Myc-NCL and grown on culture slides were fixed in 4% paraformaldehyde for 10 min at room temperature, permeabilized in 0.5% Triton X-100 for 15 min, blocked with 2% BSA in PBS for 30 min, and then incubated with anti-Myc antibody (1:500 dilution, Abmart, #M20002) for 2 h at room temperature. The slides were then washed twice in PBS before incubating in the dark with a Cy3-labelled secondary antibody (Invitrogen, #M30010) at a dilution of 1:500 in PBS with 5% BSA for 1 h. The DNA-staining marker DAPI was then used at a concentration of 1 μg/ml in the dark for 2 min. The slides were visualized with a Nikon fluorescence microscope.

Tissue IF analysis was performed according to our previous report (**Sun et al., 2015**).

Nucleoli isolation

Nucleoli were isolated according to a previously reported method (**Liang et al., 2012; Li and Lam, 2015**). Briefly, cells were washed and scraped in ice-cold solution I (0.5 ml; 0.5 M sucrose with 3 mM magnesium chloride ($MgCl_2$) and 0.2 mM PMSF). Cells were sonicated for 20 min at 30% amplitude on ice (2 s on and 5 s off) (sonicator: #JY92-IIN, Scientz, China), layered over solution II (0.7 ml; 1.0 M sucrose, 3 mM $MgCl_2$), and centrifuged at 1800 × g for 5 min at 4 ℃. The supernatant was removed carefully. The resulting pellet contained isolated nucleoli.

Transmission electron microscopy of the isolated nucleoli was performed with the standard procedure by the Microscopy Core Facility of Xi'an Jiao Tong University according to our previous report (**Wang et al., 2019**). At least 20 images were acquired for each structure of interest, and representative images are shown.

Chemicals and cell treatments

Chemicals were purchased from Sigma-Aldrich except when stated otherwise. Actinomycin D (Act D, #129935) was used at 100 ng/ml. MG-132 (#M8699) was used at 25 μM. 3-MA (#M9281) was used at 10 mM. Cycloheximide (CHX, #239764) was used at 50 μg/ml. Baf A1 (#54645, CST) was used at 0.5 μM. The above compounds were dissolved in DMSO as stock solutions before final dilution into growth medium. DMSO concentration never exceeded 1‰ (v/v). Equivalent volumes of DMSO were used as vehicle controls.

Protein expression and purification, and *in vitro* GST-H2B degradation and ubiquitination analyses

Wild-type (GST-H2BWT) and the K120R-mutated (GST-H2BK120R) H2B were cloned into the pET-42b(+) vectors and expressed as the GST-tagged form in bacteria *E. coli* (BL21) by induction with 0.5 mM (H2BWT) or 0.1 mM (H2BK120R) isopropyl β-D-thiogalactopyranoside (IPTG) for 10 h at 20 ℃. The recombinant proteins were purified using glutathione-Sepharose 4B beads at 4 ℃ overnight, then eluted with elution buffer (5 mM glutathione; 50 mM Tris-HCl, pH 8.0) for 6 h at 4 ℃ to release the protein from the glutathione-Sepharose 4B beads, and centrifuged at 2000 rpm for 5 min at 4 ℃. The supernatant was the purified recombinant protein.

The *in vitro* GST-H2B degradation and ubiquitination analyses by different cellular fractions were performed by establishing the reaction systems as indicated. The established reaction systems were then

incubated at 37 ℃ for 20 h, and the samples were directly used for Western blot analyses (degradation assays) or indirectly used for Western blot analyses after a pulldown procedure by Sepharose 4B beads (ubiquitination assays) as indicated.

4D label-free proteomic analysis

Nucleolus extracts were prepared as mentioned above. The 4D label-free proteomic analysis for the nucleolus extracts was performed by PTM Bio company (Hangzhou, China) according to its standard protocol (https://www.ptmbiolabs.com/). Briefly, the samples were firstly digested by trypsin. The protein extracts were reduced and alkylated with 5 mM dithiothreitol for 30 min at 56 ℃ and with 11 mM iodoacetamide for 15 min at room temperature in darkness respectively. The protein sample was then diluted by adding 100 mM TEAB (triethylammonium bicarbonate) to a urea concentration less than 2M. Finally, trypsin was added at 1:50 trypsin-to-protein mass ratio for the first digestion overnight and at 1:100 trypsin-to-protein mass ratio for a second 4 h-digestion. After trypsin digestion, the tryptic peptides were dissolved in 0.1% formic acid (solvent A), and directly loaded onto a home-made reversed-phase analytical column (15-cm length, 75 μm inside diameter). The gradient was comprised of an increase from 6% to 23% solvent B (0.1% formic acid in 98% acetonitrile) over 26 min, 23% to 35% in 8 min and climbing to 80% in 3 min then holding at 80% for the last 3 min, all at a constant flow rate of 400 nL/min on an EASY-nLC 1000 UPLC system. The peptides were subjected to NSI source followed by tandem mass spectrometry (MS/MS) in Q ExactiveTM Plus (Thermo, USA) coupled online to the UPLC. The electrospray voltage applied was 2.0 kV. The m/z scan range was 350 to 1800 for full scan, and intact peptides were detected in the Orbitrap at a resolution of 70,000. Peptides were then selected for MS/MS using NCE setting as 28 and the fragments were detected in the Orbitrap at a resolution of 17,500. A data-dependent procedure that alternated between one MS scan followed by 20 MS/MS scans with 15.0s dynamic exclusion. Automatic gain control was set at 5E4. Fixed first mass was set as 100 m/z. The resulting MS/MS data were subjected to database search with Maxquant search engine (v.1.5.2.8). Tandem mass spectra were searched against human uniprot database concatenated with reverse decoy database. Trypsin/P was specified as cleavage enzyme allowing up to 4 missing cleavages. The mass tolerance for precursor ions was set as 20 ppm in First search and 5 ppm in Main search, and the mass tolerance for fragment ions was set as 0.02 Da.

Chase experiment with SNAP-tagged construct

SNAP-tag is a highly engineered version of AGT (alkylguanine DNA alkyltransferase), a DNA repair

protein. 293T cells were transfected with the SNAP-tagged H2BWT (SNAP-H2BWT) for 48 h. Cells were then treated with 50 μg/ml CHX for indicated time points. Cells were harvested and lysed as mentioned above. SNAP-Cell Oregon Green substrate (#S9104S, NEB, USA) and the SNAP-H2BWT containing cell extracts reaction system were prepared according to the manufacture's instruction (https://international.neb.com/protocols/0001/01/01/labeling-of-protein-in-vitro-s9104). The reaction mixture was then incubated in the dark for 30 minutes at 37 ℃. The samples were loaded on a SDS-PAGE gel and detected using a fluorescent gel scanner in the dark.

Supplemental References

Li ZF, Lam YW. (**2015**) A new rapid method for isolating nucleoli. **Methods Mol Biol** 1228:35-42.

Liang YM, Wang X, Ramalingam R, So KY, Lam YW, Li ZF. (**2012**) Novel nucleolar isolation method reveals rapid response of human nucleolar proteomes to serum stimulation. **J Proteomics** 77:521-530.

Sun F, Xu Q, Zhao D, Degui Chen C. (**2015**) Id4 Marks Spermatogonial Stem Cells in the Mouse Testis. **Sci Rep** 5:17594.

Wang Y, Yang L, Zhang X, Cui W, Liu Y, Sun QR, He Q, Zhao S, Zhang GA, Wang Y, Chen S. (**2019**) Epigenetic regulation of ferroptosis by H2B monoubiquitination and p53. **EMBO Rep** 20(7):e47563.